

1 **A full year of continuous net soil and ditch CO₂, CH₄, N₂O
2 fluxes, soil hydrology and meteorology for a drained fen in
3 Denmark**

4 Annelie S. Nielsen¹, Klaus S. Larsen¹, Poul Erik Lærke², Andres F. Rodriguez², Johannes
5 W.M. Pullens², Rasmus J. Petersen³, Jesper R. Christiansen¹

6 ¹Department of Geoscience and Natural Resource Management, University of Copenhagen, Frederiksberg, DK-
7 2000, Denmark

8 ²Department of Agroecology, Aarhus University, Tjele, DK-8830, Denmark

9 ³Department of Ecosystems and Natural Resource Management, Aarhus University, Aarhus, DK-8000, Denmark

10 *Correspondence to:* Jesper R. Christiansen (jrc@ign.ku.dk)

11 **Abstract.** We here present a detailed dataset of automated greenhouse gas (GHG) net soil and ditch fluxes of
12 carbon dioxide (CO₂), methane (CH₄), and nitrous oxide (N₂O) from a drained fen in Denmark covering a full
13 year. The dataset resolves small scale spatial and hourly-daily-seasonal dynamics of GHG soil fluxes. The GHG
14 flux dataset is accompanied by simultaneous time series of soil temperature and moisture, as well as
15 groundwater table depth and covers spatiotemporal gradients in soil hydrological and climatic variability. The
16 GHG fluxes of CO₂, CH₄ and N₂O were measured simultaneously by a high-precision cavity ring down laser
17 spectrometer connected with a novel automated GHG system platform called SkyLine2D (Earthbound Scientific
18 Ltd., UK) that allowed up to 27 individual chamber measurement points along a 24 meter transect. In total
19 47.483 chamber measurements were completed and after quality control 44.631 CO₂ fluxes, 44.099 N₂O and
20 42.515 CH₄ fluxes remained.

21 The average (\pm SE) net soil CO₂ efflux observed at the site (2.55 \pm 0.02 $\mu\text{mol CO}_2 \text{ m}^{-2} \text{ s}^{-1}$ or 35 \pm 0.3 tCO₂ ha⁻¹ y⁻¹)
22 aligns with findings from similar drained fens in northern Europe. However, this transect average masks
23 substantial spatial variability and highlights the role of episodic emission bursts related to hydrological
24 variability. The organic soil at the site was a larger net source of N₂O (8.9 \pm 0.1 nmol N₂O m⁻² s⁻¹ or 123 \pm 1.4 kg
25 N₂O m⁻² ha⁻¹ y⁻¹) fluxes to the atmosphere compared to other temperate drained organic grassland soils in
26 northern Europe. The soil N₂O emissions measured at this site were similarly variable in space as soil CO₂
27 effluxes, but were more dynamic in time displayed a more dynamic flux behaviour than CO₂, where increasing
28 groundwater table depth in response to precipitation during warmer seasons led to emission bursts of soil N₂O
29 emissions that dominated the annual net budget of soil N₂O and decreased to near-zero fluxes in drier
30 warmer periods. Net soil CH₄ fluxes were near-zero and the site overall acted as a smaller net source
31 (0.18 \pm 0.06 nmol CH₄ m⁻² s⁻¹ or 0.91 \pm 0.3 kg CH₄ ha⁻¹ y⁻¹) compared to other drained organic grassland soils,
32 although net uptake of atmospheric CH₄ was observed as well especially in drier conditions.

33 Diurnal and seasonal patterns of net soil CO₂ and N₂O fluxes emissions align with expectations with variations
34 of soil temperature driven processes, but no clear patterns were observed for net soil CH₄ uptake or
35 emission. Compared to soil GHG fluxes, the ditch was a smaller net source of ditch CO₂ (0.94 \pm 0.05 $\mu\text{mol CO}_2$
36 $\text{m}^{-2} \text{ s}^{-1}$ or 1.3 \pm 0.7 tCO₂ ha⁻¹ y⁻¹) and N₂O (0.35 \pm 0.03 nmol N₂O m⁻² s⁻¹ or 4.9 \pm 0.4 kg N₂O ha⁻¹ y⁻¹) fluxes were 4-
37 fold and 27 fold lower, to the atmosphere respectively, while The ditch was also a net source of CH₄ (161 \pm 13
38 nmol CH₄ m⁻² s⁻¹ or 812 \pm 66 kg CH₄ ha⁻¹ y⁻¹) average of diffusive and ebullition fluxes to the atmosphere and

39 annual cumulative emissions fluxes were more than two orders of magnitude larger than net the soil CH₄
40 emissions, confirming earlier findings that ditches can be CH₄ emission hotspots, where the ditch CH₄ is emitted
41 in bursts with little seasonal variability, including emissions as ebullitions.

42 The data set (<https://doi.org/10.60612/DATADK/BZQ8JE>) set is well suited for testing and developing
43 biogeochemical models, with emphasis on the soil thermal-hydrology interactions with the peat C and N cycles.

44 **1 Introduction**

45 Understanding the climate feedbacks of temperate drained and rewetted wetlands require robust observational
46 datasets of net fluxes, e.g. whether the rewetted peatlands act as net sources or sinks of greenhouse gases
47 (GHG). This necessitates being able to capture spatial and temporal variability from these systems. Flux data
48 covering all three major GHGs are rare for temperate peatlands, and despite growing efforts to quantify GHG
49 fluxes from drained peatlands, existing datasets often suffer from limited temporal resolution, short monitoring
50 periods, or a lack of concurrent hydrological and meteorological data. Many studies rely on chamber-based
51 measurements or short-term campaigns that fail to capture seasonal dynamics and extreme events. Moreover,
52 current datasets typically offer either high temporal resolution (e.g., eddy covariance or automatic chambers)
53 with poor spatial coverage, or manual measurements with good spatial resolution but very low temporal
54 frequency. In turn this hampers the ability to model and forecast GHG fluxes, and hence climatic feedbacks, in
55 these systems under land use and climatic changes.

56 However, automated GHG closed chamber flux measurements from ecosystems are becoming increasingly
57 common, also in peatland research (Anthony and Silver 2023; Boonman et al. 2024) as equipment costs
58 decrease and awareness grows about the importance of resolving temporal variability of GHG fluxes to better
59 understand soil biogeochemical processes and soil-climate feedback. But high-frequency data of GHG fluxes
60 are still scarce for peatlands and spatial variability of fluxes is rarely represented as well due to limited number
61 of spatial replicates. Thus, most automated chamber systems are setup around a multiplexer control unit linking
62 multiple chambers with one or more GHG analysers. State-of-the-art automatic chamber systems, like the LI-
63 8250 Automated Gas Flux System (LiCOR, USA) or the eosAC-LT/LO (Eosense Inc. Canada), i.e. allow for a
64 standard number of 8 or 16 chambers, respectively, that can be upgraded to 36 chambers with additional
65 manifolds. Such large replicate chambers allow for improved characterization of spatial variation or treatment
66 effects coupled with temporal variations, but are costly to establish.

67 Additionally, the introduction of automated chamber systems raises the need for improved data handling and
68 flux calculation tailored to handle a wide range of flux magnitudes and chamber behaviour or design (Kroon et
69 al. 2008; Pihlatie et al. 2013). Recent examples of novel flux calculation software are based on publicly
70 available R codes and include goFlux (Rheault et al. 2024), HMR (Pedersen et al. 2010; Pullens et al. 2023) and
71 fluxfinder (Wilson et al. 2024). Furthermore, unsupervised automated chamber flux measurements increases the
72 likelihood of misinterpretation of fluxes, such as overestimated night-time fluxes due to atmospheric
73 stratification that disturbs the steady-state diffusion gradient between soil and the atmosphere (Brændholt et al.
74 2017) or leaky chambers that disturb chamber headspace concentrations. This is a significant challenge of
75 automated chamber systems producing thousands of data points, where manual control of each data point may
76 not be practical or feasible calling for automated and objective quality control such as used with the eddy
77 covariance methodology.

78 We here present a dataset that addresses the abovementioned limitations by uniquely combining high-frequency,
79 continuous measurements of net soil fluxes of carbon dioxide (CO₂), methane (CH₄) and nitrous oxide (N₂O)
80 with detailed hydrological and meteorological variables. The GHG fluxes were measured with an automated
81 GHG chamber system over 12 months resolving spatiotemporal patterns of GHG fluxes including 27 individual
82 collars (26 on organic soil and 1 in a ditch) over a 24 m transect on a temperate drained fen peatland. Integrated

83 quality control, flagging of erroneous or uncertain flux measurements enabled objective filtering of poor quality
84 data on the entire dataset. This comprehensive spatiotemporal coverage enables robust calibration and validation
85 of biogeochemical and hydrological models, particularly those aiming to simulate the complex interactions
86 between water table dynamics, soil processes, and GHG emissions in managed peatland systems.Flux data
87 covering all three major greenhouse gases (GHGs) are rare for temperate peatlands, and most of our
88 understanding of flux dynamics in these ecosystems are either derived from eddy covariance systems that are
89 unable to resolve small scale spatial drivers or temporally discrete manual GHG flux measurement that cannot
90 be used to understand hourly daily dynamics. In turn this hampers the ability to model and forecast GHG fluxes
91 in these systems under land use and climatic change.

92 Automated GHG closed chamber flux measurements from ecosystems are becoming increasingly common as
93 equipment costs decrease and awareness grows about the importance of resolving temporal variability of GHG
94 fluxes to better understand soil biogeochemical processes and soil climate feedback.High frequency data of
95 GHG fluxes are still scarce for peatlands and spatial variability is rarely represented as well.Most automated
96 chamber systems are setup around a multiplexer control unit linking multiple chambers with one or more
97 analyzers. State of the art automatic chamber systems, like the LI 8250 Automated Gas Flux System, allow for
98 standard number of 8 chambers that can be upgraded to 36 chambers with additional manifolds. Such large
99 replicate chambers allow for improved characterization of spatial variation or treatment effects coupled with
100 temporal variations.

101 While the basic principles and assumptions of flux calculation from static closed chamber measurements were
102 established over 40 years ago the advent of automated chamber systems raises the need for improved data
103 handling and flux calculation tailored to handle a wide range of flux magnitudes and chamber behaviour or
104 design. Recent examples of novel flux calculation software are based on publicly available R codes and include
105 goFlux, HMR and fluxfinder.

106

107 With unsupervised automated chamber flux measurements the likelihood of misinterpretation of fluxes
108 increases, such as overestimated night time fluxes or leaky chambers that disturb chamber headspace
109 concentrations. This is a significant challenge of automated chamber systems producing thousands of data
110 points, where manual control of each data point may not be practical or feasible.Integrated quality control,
111 flagging erroneous or uncertain flux measurements, enabling an objective filtering of poor quality data on the
112 entire dataset are implemented in the most recent flux calculation R scripts.Considering the critical need for
113 obtaining high-quality data on soil GHG fluxes from natural and restored peatlands in Europe and globally, our
114 dataset marks an important contribution to this endeavour as it addresses current data

115 shortcomings for Danish and European peatlands by providing detailed data on temporal and spatial patterns of
116 GHG fluxes from organic soils and drainage ditches together with environmental drivers of soil hydrology and
117 temperature, organic soil properties and groundwater geochemistry. We publish this data with the aim of it
118 being used by the scientific community for both experimentalists to test hypothesis of how GHG dynamics are
119 related to hydrology, soil, geochemistry and climate, as well as for the modelers to test and develop
120 biogeochemical models for peat lands.Integrated quality control, flagging erroneous or uncertain flux

121 measurements, enabling an objective filtering of poor quality data on the entire dataset are implemented in the
122 most recent flux calculation R scripts.

123 The objective of this study is to present a dataset on net surface fluxes of carbon dioxide (CO₂), methane (CH₄)
124 and nitrous oxide (N₂O) measured with an automated GHG chamber system over 12 months along a 24 m
125 transect on a temperate drained fen peatland. High frequency data of GHG fluxes are still scarce for peatlands
126 and spatial variability is rarely represented as well. This dataset addresses some of these shortcomings and is
127 published with the aim of it being used by the scientific community for exploring GHG dynamics in relation to
128 hydrology and climate, as well as modelling.

129

130

131 **2 Materials and Methods**

132 **2.1 Site description and the SkyLine2D system**

133 The field site, Vejrumbro ([N 56.43819 E 9.54527 \(WGS 84\)](#)), is located in Central Jutland, [in Denmark](#) near the
134 city of Viborg (Fig. 1) [with a mean annual temperature of 8.3°C and annual precipitation of 675 mm for the](#)
135 [period 1991–2020 \(measured 6 km away at Aarhus University Viborg Meteorological Station in Foulum](#)
136 (Jørgensen et al. 2023)). It is situated in the Nørre Å valley and is characterized as a riparian fen peat soil (Reza
137 Mashhadi et al. 2024). [The riparian fen developed in a former glacial river valley with flat topography gently](#)
138 [sloping \(<2.5 meters over 300 meters\) towards the Nørre Å that forms the central river in this area \(Fig.](#)
139 [S1\). Tmean annual temperature is 8.3°C with mean annual precipitation of 675 mm over the period 1991–2022](#)
140 [\(Aarhus University Viborg Meteorological Station, Foulum\)](#). The site was drained in 1950 with ditches and tile
141 drains for cultivation but has primarily served as grassland in recent decades due to the wet conditions (Nielsen
142 et al. 2024). [The riparian fen developed in a former glacial river valley with flat topography gently sloping \(<2.5](#)
143 [meters over 300 meters\) towards the Nørre Å that makes out the central river in this area \(Fig. 2\). Farming](#)
144 [practices with tillage and crops stopped approximately 20 years ago after which it was managed as a harvested](#)
145 [grassland](#). Since 2018, Vejrumbro has been a living lab for agroecological research managed by the Department
146 of Agroecology at Aarhus University. From 2018, the site had a passive rewetting strategy by terminating
147 maintenance of the open ditches. During 2022, the main ditches were gradually blocked. [Currently, the area is](#)
148 [being encroached by *Juncus effusus* except in few plots of the field where paludiculture research is taking place](#)
149 ([Nielsen et al. 2024\)](#).

150 **2.1.1 Site preparation and disturbance**

151 [Initially, we chose to perform the flux measurements without aboveground plants as the small chamber](#)
152 [dimensions \(height of 20 cm\) prohibited inclusion of these in the chamber as the plants typically reach over 100](#)
153 [cm in height at this site. The strategy was therefore to focus on measuring net soil GHG fluxes, where we](#)
154 [assume the contribution of gases are derived from heterotrophic respiration of older peat C/N, root exudated](#)
155 [C/N from adjacent plants, dissolved N in groundwater and belowground autotrophic respiration \(CO₂\) from](#)
156 [roots inhabiting the peat below the collars. We are aware that omitting plants prohibit a full evaluation of the net](#)
157 [ecosystem exchange of GHG and hence its net climate impact, as the aboveground plants represent a net sink of](#)
158 [atmospheric CO₂ and also can increase the emission of CH₄ and N₂O \(Jørgensen et al. 2012; Vroom et al. 2022\).](#)

159 [However, by avoiding plants we also isolate the soil processes leading to net soil emission/uptake of the GHG](#)
160 [and resolve spatiotemporal patterns to a higher degree than previous studies at this site have achieved and what](#)
161 [other commercial platforms are capable of. Collectively, this can provide a mechanistic insight into the](#)
162 [regulation of fluxes by hydrology and temperature. We acknowledge that future studies of GHG fluxes in](#)
163 [peatlands should seek to include the aboveground plant component to the net GHG flux from the ecosystem.](#)

164 [The disturbance to the transect related to initial harvesting and removal of aboveground plants and continuous](#)
165 [removal of aboveground live plant inside the collars and in a small perimeter outside the collar. In this way we](#)
166 [kept an approximate area of 40 x 40 cm clear of vegetation at each collar. Two months prior to installation of](#)
167 [collars in summer of 2021, the transect \(Fig. 2\) was harvested and remaining living aboveground vegetation was](#)
168 [killed by applying one recommended dose of glyphosate \(~100 mg m⁻²\) to the plants only across the transect and](#)

169 avoiding spraying on the soil surface. The half-life of labile glyphosate in mineral soils range between 6-87 days
170 (average 21 days) (Padilla and Selim 2020) with clay contents increasing half-life. The absence of clay and low
171 dosage indicate that there were no, or only little traces of glyphosate left once the flux measurements began and
172 hence the glyphosate treatment likely did not have a direct impact on the measured fluxes. Continued glyphosate
173 application would potentially have reduced microbial activity in the soil and thus lower microbial respiration
174 (Nguyen et al. 2016). Considering that we sprayed the vegetation only one time with glyphosate months prior to
175 flux measurements, we assume the direct impact on soil microbial processes to be small. However, we cannot
176 fully rule out that glyphosate may have led to a transient response. Because we did not have an undisturbed
177 control we cannot quantify the effects of glyphosate. Subsequently, regrowth inside the collars was restricted by
178 manual harvesting of emerging plants at a minimum of once every 7 days and throughout the period. Plant
179 removal from collars is considered a common practice to isolate net soil GHG fluxes as the aboveground
180 autotrophic respiration is removed. Since the individual collars were not trenched it is unavoidable to include
181 belowground autotrophic respiration from plants growing adjacent to the collars. To avoid excessive disturbance
182 of the site we did not remove these roots. Since we did not have a control, untreated/unharvested plot it is not
183 possible to assess the direct impact of the disturbance on the GHG fluxes.



184
185 Figure 14: The Vejrumbro location in Jutland (N 56.43819 E 9.54527 (WGS 84)) in the Nørre Å valley near the
186 village of Vejrumbro. The grey circle marks the placement of the SkyLine2D system. Satellite images: © Google
187 Earth.

188 [2.1.2 Peat and organic soil characteristics](#)

189 In November 2023 the peat across the SkyLine2D transect was sampled to 1 meter depth using a Russian auger
 190 and cores split into five layers of 20 cm thickness. Collars 1, 2, 5, 6, 8, 13 – 27 were sampled. For the remaining
 191 collars it was not possible to retrieve a sample due to excessive wetness of the peat. The decomposition of the
 192 peat samples were assessed by a 10-point Von Post scale of humification (1 = completely undecomposed and 10
 193 = completely decomposed) together with quantification of the pH_{H₂O} (1:5 peat:water mix), dry bulk density (g
 194 cm⁻³) and total C and N by dry combustion (g C/N 100 g peat⁻¹ or %) (Table 1).

195 **Table 1 Mean (±standard error of the mean (SE)) peat/organic soil characteristics of humification degree (Von Post),**
 196 **pH (H₂O), dry bulk density (ρ_{dry}), total C (TC) concentration, total N concentration (TN) and the C/N ratio for collars**
 197 **1, 2, 5, 6, 8 and 13 - 27 at the Vejrumbro transect.**

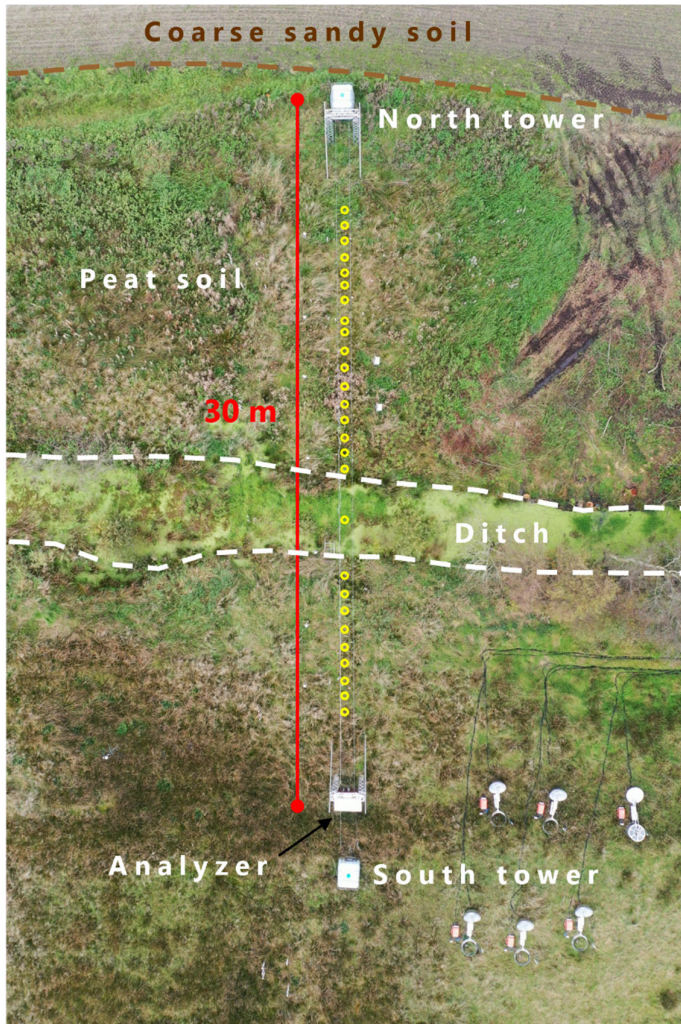
Depth (cm)	N	Von post		pH (H ₂ O)		ρ _{dry} (g cm ⁻³)		TC (%)		TN (%)		C/N	
		Min	Max	Mean	±SE	Mean	±SE	Mean	±SE	Mean	±SE	Mean	±SE
0-20	20	7	10	4.2	0.08	0.31	0.02	26	1.1	1.6	0.06	16	0.4
20-40	20	5	10	4.6	0.06	0.20	0.01	43	1.3	1.8	0.04	24	0.7
40-60	11	3	8	4.9	0.10	0.15	0.01	48	1.8	1.9	0.05	25	1.1
60-80	11	3	6	5.3	0.09	0.11	0.01	47	1.8	1.9	0.05	24	0.6
80-100	10	1	8	5.4	0.09	0.10	0.02	44	2.1	1.9	0.05	24	0.6

198 Generally, there was peat/organic soil to one meter depth except for one collar (25) where gyttja was found in a
 199 depth of 80 cm (Table 1). The organic soil was more decomposed in the top 40 cm indicated by higher Von Post
 200 values between 5 and 10. Below 40 cm peat still displayed high levels of decomposition along the transect, but
 201 was more often found to be less decomposed, values ranging from 1-8 (Table 1). This corresponds well to the
 202 previous land use with drainage of the topsoil leading to higher degree of humification. Also, the organic soil
 203 was most dense in the top 20 cm (on average 0.31±0.02 g cm⁻³) and bulk density decreased to 0.10 – 0.12 g cm⁻³
 204 from 40 – 100 cm depth. Total C and N was lowest in the 0-20 cm layer, but still classified as organic soil.
 205 Below 20 cm total C and N concentrations, respectively were similar. C/N ratio was lowest in the top 20 cm
 206 (16±0.4) and increased to 22-25 in 20 – 100 cm depth (Table 1).

207 2.1.3 Groundwater water sampling and chemical analysis

208 Groundwater was sampled monthly in the piezometers placed at collars 1, 5, 13, 18, 22 and 27 (Fig. 3) by
 209 retrieving a 200 mL sample 20-30 cm below the groundwater level at the sampling time. The water sample was
 210 retrieved using a syringe and transferred to a plastic bottle that was capped to avoid air bubbles. Water samples
 211 were frozen immediately after sampling and subsequently after thawing analyzed for pH, EC and alkalinity on a
 212 855 Robotic Titrosampler (Metrohm, Germany). Total N and DOC were measured on a TOC-V CPH Analyzer
 213 with Total Nitrogen Unit TNM-1 & ASI-V Autosampler (Shimadzu, Japan). Ion chromatograph (IC) analyses
 214 of Cl⁻, NO₃⁻, and SO₄²⁻ were performed on a 930Compact IC Flex (Metrohm, Germany) and NH₄⁺
 215 concentrations were measured with continuous flow analysis using a Seal AA500 Autoanalyzer (SEAL
 216 Analytic, USA). Total dissolved Fe and P were analyzed with coupled plasma–mass spectrometry (ICP-MS) on
 217 an iCAP-Q ICP-MS (Thermo Fisher Scientific, USA) in KED mode using He as the collision gas. Prior to
 218 analysis the 10 mL subsamples were acidified with 200 μ L concentrated nitric acid to a 10 mL sample.
 219 Elemental ICP-MS analyses also included dissolved base cations of Ca²⁺, Mg²⁺, K⁺, Na⁺ as well as total
 220 dissolved Al and Mn cations (not shown, but included in the data set).

221



222

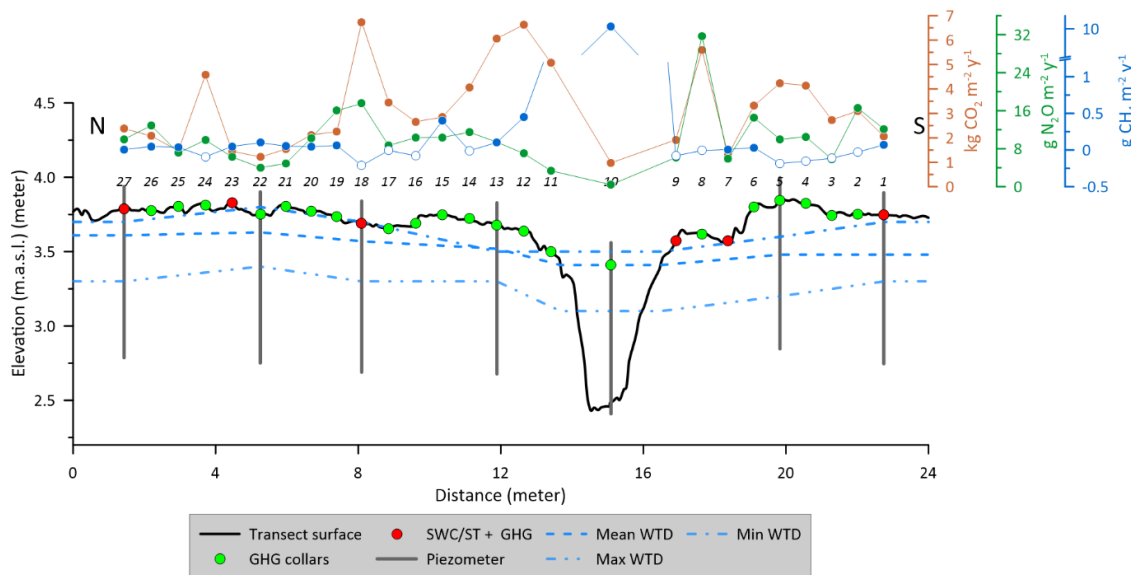
223 Figure 23: Drone image of the measurement transect (September 27th 2023) after flux measurements had stopped.
 224 Dashed brown line marks the approximate boundary between the agricultural field, coarse sandy soil (JB-nr. 1
 225 according to the Danish soil classification (north)) and the peat/organic-soil (JB-nr. 11 according to the Danish soil
 226 classification (south)). The red line marks the end points of the SkyLine2D system (30 meters). The open yellow
 227 circles (n=27) mark the approximate position of individual collars across the transect of the field (22-24 meters in
 228 length) where greenhouse gas fluxes were measured. The ditch is placed between indicated with the dashed white
 229 lines. The analyser was placed at the south tower. Elevation above sea level along the 22-24 meter collar transect
 230 varied little across the transect from 3.77 m in the south to 4.06 m in the north.

231 2.1.4 SkyLine2D system configuration at Vejrumbro

232 The SkyLine2D system is an automated chamber based system for measuring GHG fluxes. The system is
 233 designed and built by Earthbound Scientific Ltd. (England United Kingdom). We used the SkyLine2D system to
 234 measure the net soil fluxes of carbon dioxide (CO₂), methane (CH₄) and nitrous oxide (N₂O) measured with an

235 automated GHG chamber system over 12 months resolving spatiotemporal patterns of GHG fluxes including 27
236 individual collars (26 on organic soil and 1 in a ditch) over a 24 m transect on a temperate drained fen peatland.

237 The SkyLine2D measurement system transect was oriented in an N-Snorth-south direction (Fig. 32). Two 2.5
238 meter-tall scaffold towers marked the end of the 30 m SkyLine2D system (Fig. 23 and Fig. 5DS2D). The towers
239 were fixed by ropes attached to 1000L pallet tanks filled with water (Fig. 5DS2D) that maintained a stable
240 position of the towers and ropes and hence placement of the chamber over the collars. The measurement transect
241 was in total 22-24 m with 27 individual measurement collars for GHG fluxes on the ground, 26 on peat+organic
242 soil and 1 in a drainage ditch (Fig. 32 and 43). The GHG analyser (model G2508, Picarro Inc., USA) was
243 installed in a waterproof and temperature-controlled shelter at the south end of the transect (Fig. 32 and Fig.
244 5BS2C). The transect was situated on the edge of the riparian fen in close proximity to the mineral upland soils,
245 where active agriculture was practiced (Fig. 32). Along the transect volumetric soil water content (SWC) and
246 soil temperature (ST) as well as water table depth (WTD) was-were measured at seven locations along the
247 transect (Fig. 4). The farmer's agricultural field north of the SkyLine2D was sown with annual crops in rotation
248 according to normal practice.



249
250 **Figure 34: Schematic representation of the measurement transect at Vejrumbro and associated measurement**
251 **variables.** The annual cumulative fluxes of CO_2 (red) ($\text{kg CO}_2 \text{ m}^{-2} \text{ v}^{-1}$), N_2O (green) ($\text{g N}_2\text{O m}^{-2} \text{ v}^{-1}$) and CH_4 (blue) (g
252 $\text{CH}_4 \text{ m}^{-2} \text{ v}^{-1}$) are shown for each collar across the measurement transect at Vejrumbro. Closed and open symbols for
253 CH_4 represent net cumulative emission and uptake, respectively. Mean WTD is the mean water table depth
254 measured in piezometers (blue dashed line). GHG collars (green symbols) mark the positions of greenhouse gas flux
255 measurements of CO_2 , CH_4 and N_2O . SWC/ST + GHG mark the positions where volumetric soil water content
256 (SWC) and soil temperature (ST) at 5 cm depth were measured alongside greenhouse gas fluxes. Numbers on top of
257 plot show the collar numbers (from 1 – 27). N and S mark the north and south ends of the transect (see Fig. 3). The
258 peat depth was at least one meter in all points. The lower depth of peat in the diagram is however arbitrary.

259 2.2 Overview of Data variables time series of GHG fluxes, soil temperature/moisture, air temperature, wind
260 direction and groundwater level

261 The dataset is comprised of a ~~1312~~-month time series of net soil fluxes of CO₂, CH₄ and N₂O, accompanied by a
262 longer timeseries of soil temperature and moisture at 5 cm depth, meteorological variables (air temperature,
263 wind speed and direction measured at 2 meter height) and a shorter time series groundwater table level, depth
264 and temperature (Fig. 43, Table 42). Due to equipment failure of the SkyLine2D the GHG flux measurements
265 started on ~~August 1st 2021, with a data gap between September 1st 2021 and February 1st 2nd, 2022 due to~~
266 ~~equipment failure~~ (Table 42). Groundwater level measurements started between March 9th to 31st 2022 (Fig. 4,
267 Table 1). All other variables were measured continuously from July 1st 2021, until ~~January~~ January 31st
268 2023 (Fig. 4, Table 1). In the period between December 7th and 19th, 2022 intermittent periods of snow cover
269 (depth was not measured) on the ground occurred. This snow cover did not impede flux measurements.

Table 234: Available time series data from the Vejumbro SkyLine2D system. Coloured time periods in 2021 to 2023 for each variable indicate data availability.

Variable	Unit	Model/sensor type	Data availability												2023						
			2021			2022			2023												
			Aug	Sep	Oct	Nov	Dec	Jan	Feb	Mar	Apr	May	Jun	Jul	Aug	Sep	Oct	Nov	Dec	Jan	
CO ₂ flux ⁺	μmol CO ₂ m ⁻² s ⁻¹	G2508 (Picarro Inc., USA)	~10 ^{**2}																		
CH ₄ flux ⁺ lux [*]	nmol CH ₄ m ⁻² s ⁻¹	G2508 (Picarro Inc., USA)	~10 ^{**2}																		
N ₂ O flux ⁺	nmol N ₂ O m ⁻² s ⁻¹	G2508 (Picarro Inc., USA)	~10 ^{**2}																		
Soil temperature at 5 cm depth ^{**3}	°C	RXW-TMB-868 (Onset, USA)																			
Soil water content at 5 cm depth ^{**3}	(cm ³ cm ⁻³)	RXW-SMD-868 (SHS) (Onset, USA)																			
Air temperature at 2 m height	°C	S-TIC-M002 (Onset, USA)																			
Wind speed	m s ⁻¹	S-WSB-M003 (Onset, USA)																			
Wind direction	°	S-WDA-M003 (Onset, USA)																			
Groundwater level ^{**4} depth ^{***}	m.a.s.l.	DCL532 (BD sensors, Germany)																			
Groundwater table depth ^{***}	cm	DCL532 (BD sensors, Germany)																			
Groundwater temperature ^{**}	°C	Dallas DS 18B20																			

⁺Net^{*} Net soil/ditch fluxes for all collars 1 - 27.^{**}Time in between two consecutive flux measurements. The 10 minutes comprise actual flux measurement of 5 minutes and 5 minutes headspace flushing between flux measurements.^{**3}Measured for a subset of collars: 4, 7, 9, 18, 23, 27.^{**4}Measured for a subset of collars: 1, 5, 10 (ditch), 13, 18, 22, 27.

276 **2.3 Soil moisture and temperature measurements**

277 Soil moisture was measured at collars 1, 7, 9, 18, 23, 27 (Figure 4) and probes (6 cm length) were inserted at an
278 approximate 30° angle 5 cm outside the collar, while the soil temperature probes were inserted vertically
279 adjacent to the soil moisture probe.

280 **2.4 Groundwater table level and depth**

281 Piezometers (inner diameter 5 cm) were installed -at collars 1, 5, 10 (ditch), 13, 18, 22, 27installed (Figure 4) to
282 1 meter depth below the surface, which is deeper than the lowest groundwater level in summer (~60 cm below
283 the surface) with openings from 0.1 – 1.2 meter below terrain. In the ditch the piezometer bottom was deeper
284 than one meter to secure anchoring in the peat. The piezometers were installed approximately 50-60 cm beside
285 the collars to avoid interference with the SkyLine2D system. After installation, piezometers were cleaned and
286 sealed at the surface with bentonite pellets to avoid surface infiltration along the piezometers which can distort
287 water level measurements.

288 Pressure transducers (DCL532, BD Sensors, Germany)(Table 2) connected to Arduino-loggers were installed in
289 each piezometer (at collars 1, 5, 10, 13, 18, 22 and 27 – Fig. 35) approximately 1 m below terrain collecting
290 measuring water levels every 15 minutes. The pressure transducers were vented, andvented and thus do not need
291 correction for atmospheric pressure.

292 The groundwater levels were described using two metrics: hydraulic head and groundwater depth (GWD).
293 Hydraulic head represents the water level relative to mean sea level, based on the Danish Vertical Reference
294 (DVR90), while GWD indicates the depth of the groundwater below the surface terrain. The elevation of top of
295 the piezometers were measured using a GPS (model GS07 High Precision GNSS Antenna with a CS20
296 Controller, Leica, Germany) and used as a local reference for hydraulic head. Manual measurements of
297 groundwater levels were conducted every 2 months and used to calibrate the logger water levels to hydraulic
298 head and GWD.

299 **2.5 Wireless data transfer**

300 Wireless sensors for air temperature, wind speed, wind direction, soil temperature and volumetric soil water
301 content were set up with Wi-Fi data transfer to HOBO RX3000 Weather Station (Onset, USA) equipped with
302 HOBOnet Manager (RXMOD-RXW-868) module for wireless communication with sensors and logged data
303 every 5 minutes. Data access was through the HOBOlink cloud software.

304 Groundwater loggers were interfaced with the I²C (Inter-integrated Circuit) protocol and data was collected on
305 Arduino custom-built logger (<https://vandstande.dk/logger.php>) with wireless connection via LoRaWAN or
306 SigFox.

307 **2.6 Greenhouse gas flux measurements with the**

308 **2.6.1 SkyLine2D system -at Vejrumbro**

309 The SkyLine2D system is designed and built by Earthbound Scientific Ltd. (England). The SkyLine2D system
310 is designed and built by Earthbound Scientific Ltd. (England) Along the SkyLine2D transect the 27-26 individual

311 collars (\varnothing 19 cm) along the 22-24 meter transect on organic soil (Fig. 3) were inserted 5 cm into the peat leaving
312 5 cm above the surface. The collars were distanced app. 70 cm apart. +One collar was installed in the ditch by
313 inserting a tube (\varnothing 19 cm, length 100 cm) to the bottom of the ditch with holes deeper than the minimum water
314 level in the ditch to allow water flow. Thus, it was avoided that air entered in the collar in the ditch due to low
315 water levels in the ditch. On top of this longer tube a collar (\varnothing 19 cm, length 10 cm) was glued to the top
316 allowing for flux measurements. The chamber was programmed to stop when the bottom of the chamber hit sat
317 the water surface if the water level in the ditch extended above the top of the collar. For the majority of
318 most of the time the collar was not submerged and the chamber therefore hit the collar.

319 Prior to installation of collars in summer of 2021, the transect (Fig. 3) was harvested and remaining living
320 aboveground vegetation was killed by applying one dose of Glyphosate across the transect. Subsequently,
321 regrowth inside the collars was restricted by manual harvesting of emerging plants at a minimum of once every
322 7 days and throughout the period. Thus, the fluxes measured represent the net soil GHG flux.

323 **2.6.2 Trolley and Chamber**

324 There was one round transparent chamber (height: 39.5 cm and inner \varnothing : 19 cm, volume: 11.2 L) on the
325 SkyLine2D, hanging below a moving trolley, which was suspended on two ropes stretched between the north
326 and south towers (Fig. 5A-S2A and B). At defined positions along the rope, neodymium magnets had been
327 inserted, and a magnet sensor (Fig. 5B-S2B) on the trolley informed the internal computer to stop and lower the
328 chamber over positions with a collar on the surface. The chamber was lowered and guided down to the collar by
329 supporting rods shaping a funnel (Fig. 5A-S2A). The chamber stopped when it hit the collar, achieved through a
330 pressure sensor on top of the chamber connected to a hollow rubber gasket (\varnothing 3 cm) at the bottom, which also
331 sealed the chamber with the collar. There was no fan installed in the chamber as the mixing was ensured by the
332 main pump (Fig. 5C-S2C). A vent was installed in the top of the chamber to allow for pressure equilibration
333 under windy conditions and chamber deployment.

334 Two signals from the internal computer in the trolley were logged on the RMX3000 datalogger during the time
335 the chamber was on the collar: chamber closed (CH_closed) and chamber ID (CH_ID). CH_closed measured
336 the cumulative time the chamber was in contact with the collar, while CH_ID was recorded as a voltage output
337 dependent on the magnet number, starting with 0.05V for CH_ID 1. With 30 magnets in the rope, the maximum
338 CH_ID value was 1.5. In this study, 27 out of the 30 magnets were used. One entire flux + flushing sequence
339 lasted 10 minutes (Table 1). The chamber closure period was set to 5 minutes with a purging time of 5 minutes
340 in between measurements when chamber was open and hanging underneath the trolley at approximately 1 meter
341 above the ground (Fig. S2D). This provided on average 10 min between flux measurements on consecutive
342 collars (Table 1). Due to small variations in mechanical operations, flux measurements were occasionally farther
343 apart than 10 minutes, but overall, the timing of the SkyLine2D system was consistent. After each cycle of 27
344 flux measurements there was a 30-minute delay until the start of the next cycle. On average this resulted in 4-5
345 flux measurements per collar per day throughout the period.

346 To determine the concentrations of CO₂, CH₄ and N₂O in the chamber air, a laser spectroscopy GHG analyser
347 (model G2508, Picarro Inc., USA) was used. The sample output frequency was set to 1 Hz with a manufactured
348 specified raw precision on 1 Hz data for CO₂: 240 ppb, CH₄: 0.3 ppb and N₂O: 5 ppb at ambient conditions

349 (Picarro Inc., USA). A main pump (model: N86 KN.18, KNF, Germany) circulated the air to and from the
350 chamber at 6 L min^{-1} . The GHG analyser was installed in parallel to the inflow from the chamber due to the
351 much lower flow of 250 mL min^{-1} of the vacuum pump. There was a 30-meter tube between the chamber and
352 main pump to allow for the GHG analyser to remain stationary in the hut while the trolley moved.

353

354

355 **Figure 5: A)** The SkyLine2D trolley and chamber at Vejrumbro site looking from south towards the north tower.
356 Note the orange collars on the ground arranged in a straight line. **B)** Close up of the chamber: wheels move the
357 trolley back and forth on the ropes (1), magnet sensors (2) and rubber gasket on the bottom of the chamber (3). **C)**
358 The analyzer “hut” with the Picarro G2508 gas concentration analyzer (4) and the main pump (5). **D)** The SkyLine2D
359 system with the north and south towers and the analyzer shelter. Towers were at both ends attached with ropes to
360 water-filled 1000 L pallet tanks. One tank shown at the right of the picture.

361

2.6.3 Flux measurements

362 One entire flux + flushing sequence lasted 10 minutes (Table 1). The chamber closure period was set to 5
363 minutes with a purging time of 5 minutes in between measurements when chamber was open and hanging
364 underneath the trolley at approximately 1 meter above the ground (Fig. 5D). This provided on average 10 min
365 between flux measurements on consecutive collars (Table 1). Due to small variations in mechanical operations,
366 flux measurements were occasionally farther apart than 10 minutes, but overall the timing of the SkyLine2D
367 system was consistent. After each cycle of 27 flux measurements there was a 30 minute delay until the start of
368 the next cycle. On average this resulted in 4-5 flux measurements per collar per day throughout the period.

369 To determine the concentrations of CO_2 , CH_4 and N_2O in the chamber air, a laser spectroscopy analyzer (model
370 G2508, Picarro Inc., USA) was used. The sample output frequency was set to 1 Hz with a manufactured
371 specified raw precision for CO_2 : 240 ppb, CH_4 : 0.3 ppb and N_2O : 5 ppb at ambient conditions (Picarro Inc.,
372 USA).

373 A main pump (model: N86 KN.18, KNF, Germany) circulated the air to and from the chamber at 6 L min^{-1} . The
374 G2508 gas analyzer was installed in parallel to the inflow from the chamber due to the much lower flow of 250
375 mL min^{-1} of the vacuum pump. There was a 30-meter tube between the chamber and main pump to allow for the
376 analyzer to remain stationary in the “hut” while the trolley moved. This unavoidably created a delay in the
377 chamber headspace GHG concentration of about 60 seconds after chamber closure.

378

The analyzer, vacuum pump and main pump were placed in an automatically ventilated wooden “hut” (Fig. 5C).
379 An overview of the SkyLine2D system in place is shown in Fig. 5D.

380

2.7 Calculation of diffusive fluxes

381 Fluxes were calculated and quality checked using the procedure outlined in the goFlux R package (Rheault et al.
382 2024) and presented as $\mu\text{mol CO}_2 \text{ m}^{-2} \text{ s}^{-1}$, $\text{nmol N}_2\text{O m}^{-2} \text{ s}^{-1}$ and $\text{nmol CH}_4 \text{ m}^{-2} \text{ s}^{-1}$. The CO_2 , CH_4 and N_2O
383 concentrations in ppm were converted to moles using the ideal gas law.

384 Prior to flux calculations, the gas concentration data from the G2508 was matched to the [chamber closure time](#)
385 [and chamber id](#)~~CH~~[closed and CH_ID time series](#) in order to determine the start time of the chamber
386 measurement, so it was possible to separate individual flux measurements from each collar over the
387 measurement time (see examples of flux detection and calculation in Fig. [6AS3A-D](#)). An automatic deadband
388 detection method was applied based on maximal R^2 of a linear regression over the first 180 s (in 10 s steps) after
389 chamber closure. The deadband was allowed to attain values between 0 to 150 seconds thereby also allowing for
390 compensation for the ~60 s delay between chamber headspace gas concentration change and [G2508-GHG](#)
391 [analyzer](#)~~analyser~~ detection due to transport time through the 30 m tube connecting the chamber and [GHG](#)
392 [analyzer](#)~~analyser~~.

393 Flux calculations were done with both linear (LM) and non-linear (Hutchinson-Mosier – HM) regression models
394 (Pihlatie et al. 2013) to determine the slope at time zero. The best flux ~~estimate~~[estimates](#) with either the LM or
395 HM regression model was determined using the *best.flux* function in the goFlux package (Rheault et al. 2024).
396 Shortly, if the RMSE of the HM model was lower than minimum detectable flux (MDF), HM was chosen.
397 However, if the ratio (g-factor) between HM and LM was larger than 2, LM was chosen, as this indicates over-
398 fitting of the HM, which may result in unrealistic large HM flux estimates. If the relative SE of the slope
399 (SE/slope) at time zero for the HM model was larger than 100% ~~than the SE of the LM it also indicated~~
400 overfitting [of the HM model](#) and the LM was chosen. This approach is conservative as it will discard non-linear
401 flux behaviour and instead provide a conservative linear flux estimate. Out of 47.438 detected flux
402 measurements for CO₂, CH₄ and N₂O, respectively, a total of 2807 CO₂ fluxes (5.9%), 3339 N₂O fluxes (7%)
403 and 4923 CH₄ fluxes (10.3%) were discarded [either](#) due to chamber mechanical malfunction (imperfect sealing
404 on collar [due to](#)~~or~~ erroneous lowering of chamber on collar [indicated by background atmospheric or fluctuating](#)
405 [gas concentrations in the headspace](#)~~)-~~. [At low flux levels non-significant fluxes](#) ~~were discarded as it was not~~
406 [possible to visibly detect whether there was a flux due to high noise-signal ratio of the analyser and/or it was](#)
407 [because the chamber had malfunctioned](#)~~and non significant regression due to noisy measurements at low flux~~
408 [levels](#). [It is acknowledged that discarding low fluxes can bias annual means and cumulative values, but the data](#)
409 [quality did not allow us to determine whether the flux measurement was performed correctly and hence a](#)
410 [conservative approach was chosen as including false low fluxes would also bias the data set](#).

411 For flux measurements the air temperature in 2 meters was used as an estimate of the chamber headspace
412 temperature along with a 1 atm air pressure.

413 The annual [budget of cumulated](#) fluxes from the soil or the ditch ~~was~~[were](#) estimated simply by multiplying the
414 daily average CO₂, CH₄ or N₂O flux for the measurement period with 365 days. We believe for the purpose of
415 data presentation that this simplistic methodology is adequate here, also given the very few data gaps in the
416 timeseries. However, there are other more sophisticated methods using interpolation and response variable
417 functions that may refine the annual budget. However, it is not the goal of this manuscript to present these
418 methodologies but to provide the data so other users can test different temporal upscaling methodologies.

419

420 [Figure 6: Example of flux detection and resulting flux calculation using linear \(blue\) \(LM\) and non-linear \(red\) \(HM\)](#)
421 [regression models. Chamber closure is marked by the black vertical line and the 120 second flux calculation window](#)

422 marked by the green vertical lines. Examples of successful measurements of A) net CH₄ uptake measurement, B) CO₂
423 efflux, C) example of erroneous detection of chamber closed and D) example of measurement of non-detectable N₂O
424 flux with HM overfitting.

425 Due to a combination of variability in flux magnitudes and the mechanics of the SkyLine2D it is possible to
426 achieve a number of situations where fluxes will be discarded. Successful flux measurements and calculations
427 are when the timing of chamber closed and GHG time series are synchronized (Fig. 6A and B). As seen from
428 the numbers in the previous paragraph this was the case in more than 90% of all flux measurements. However, if
429 there was a mismatch between the chamber closed detection and the time series of GHG concentrations the flux
430 would be calculated on a wrong “window” of the actual enclosure (example in Fig. 6C). This window could
431 either be too early or late and fluxes would accordingly be discarded. Lastly, at low fluxes, but otherwise
432 successful deployment of the chamber, the HM model could overfit the GHG time series and result in unrealistic
433 flux estimates (Fig. 6D). In this case flux calculations would also be discarded.

434 2.8 Calculation of ebullition fluxes in the ditch

435 Methane Ebullition flux, e.g. mass flow of CH₄, was occasionally observed only in the ditch. The
436 resultant CH₄ time series for the chamber would have a characteristic appearance (Fig. 7S4) where the
437 measurement would essentially start out as diffusive flux measurement, then CH₄ bubbles entered the chamber
438 headspace, and the concentration would quickly increase to a maximum value and reach a threshold
439 concentration corresponding to the mixed headspace concentration. In these cases, the LM/HM flux
440 calculation assumptions are violated and instead the ebullition flux would be calculated as the total increase in
441 CH₄ mass m⁻² per 5 min enclosure⁺. The mass flux of CH₄ per enclosure (nmol m⁻² per 5 min enclosure⁺) was
442 calculated according to Eq. (1):

$$443 F_{CH_4-ebu} = dCH_4 * \frac{V_{system}*P}{A*R*T} * 10^{-6} \quad (1)$$

444 Where dCH₄ is the concentration difference in nmol between start of chamber enclosure (CH_{4,start}) and end CH₄
445 concentration (CH_{4,end}) after it reached a plateau (Fig. 7S4), V_{system} is the total volume (11.7 L) of the system
446 (collar, chamber, tubes and GHG analyzer) in L, P is the pressure (1 atm), A is the area of the collar
447 (0.028 m²), R is the gas constant (0.082057 L atm K⁻¹ mol⁻¹) and T is the chamber headspace temperature (K).
448 The time step of dCH₄ was assumed to be 1 second meaning that the flux unit is nmol CH₄ m⁻² s⁻¹.

449 As the fluxes from the ditch were only measured 4-5 times per day (every 5-6th hour), the measured ebullition
450 fluxes were upscaled to daily basis under the assumption that the frequency of ebullitions were constant during
451 24 hours. This may not be the case as ebullition fluxes from open water surface are known to be erratic.
452 However, ebullition would happen also from the ditch when the flux was not measured, so upscaling ebullition
453 on a daily basis is the best estimate. Out of a total of 1728 flux measurements from the ditch (collar 10), 334
454 were classified as ebullitions indicating that ebullition was erratic which is in line with studies of ebullition of
455 fluxes from ponds (Wik et al. 2016; Sø et al. 2023). Hence, it can be assumed that ebullition occurred around
456 19.3% of the time during the measurement period (360 days). Furthermore, the ebullition flux is calculated as
457 the accumulated CH₄ in the chamber headspace during the entire flux measurement, e.g. 5 minutes (Sø et
458 al. 2023), and the calculated ebullition flux in the data set is therefore representative of 5 minute enclosure and

459 not per second. To extrapolate to an annual estimate the number of 5 minute enclosures in 19% of 360 days is
460 therefore estimated ($N=20049$ 5-min 360 days $^{-1}$), multiplied with the average ebullition flux (nmol CH₄ m $^{-2}$ 5
461 min $^{-1}$). The total ebullition flux from the ditch was upscaled to daily basis by multiplying the daily average
462 measured ebullition flux per enclosures of 5 min with the number of possible 5 min enclosures in 24 hours (e.g.
463 24*60/5).

464 For example on April 6th 2022 two ebullition fluxes were calculated (538 and 266 nmol CH₄ m $^{-2}$ 5 min $^{-1}$;
465 average of 402 nmol CH₄ m $^{-2}$ 5 min $^{-1}$). To upscale to a daily basis the average value was multiplied by the
466 number of 5 min enclosures in 24 hours, e.g. 402*24*60/5 = 115822 nmol CH₄ m $^{-2}$ d $^{-1}$.

467 **Figure 7: Example of ebullition measurement in the chamber.**

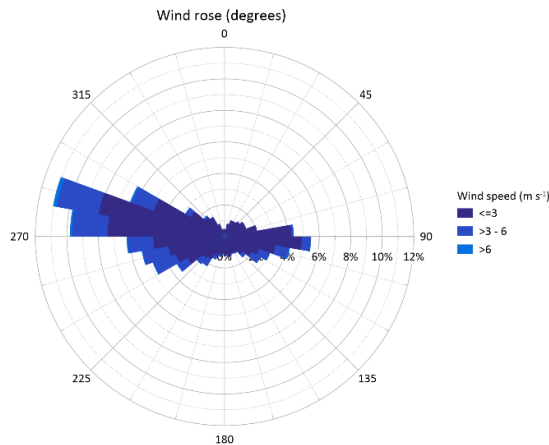
468 Ebullitions could also be caused by mechanical disturbance of the chamber landing on the collar. Ebullition
469 fluxes were discarded if the sudden increase in CH₄ headspace concentration (Fig. 7S4) occurred 30 seconds
470 after recorded chamber closure as this indicated bubbles released by chamber deployment on top of the collar.

471

472 **3 Data presentation**

473 **3.1 Wind speed and direction**

474 Generally, the wind ~~elimate regime~~ during the measurement period was rather mild with monthly average wind
475 speeds ranging between 1.2 to 2.9 m s⁻¹ and maximum gust up to 20 m s⁻¹ (Fig. 8A). ~~There was a typical~~
476 ~~seasonal behaviour of wind speed from winter to summer and an increase again towards the autumn (Fig. 8A) as~~
477 ~~is typically experienced in Denmark~~. The wind direction was uniformly from the west for 52% of the time, with
478 easterly winds constituting 27% and northern and southern winds 8 and 13% of the time (Fig. 8A). Winds from
479 western directions were highest for the longest ~~period of time~~, while easterly winds were of similar
480 magnitude, but less frequent (Fig. 8B). Northern and southerly winds were generally below 3 m s⁻¹ and
481 represented periods with still conditions. ~~The dominance of direction and magnitude from a western direction is~~
482 ~~in line with the general wind direction in Denmark~~. The very uniform western-eastern wind field at Vejrumbro
483 may also partly be explained by the W-E direction of the valley in which the site is situated, that effectively
484 blocks or dampens winds from S and N.



485

486 **Figure 48: Wind ~~elimate regime~~ at Vejrumbro for the period July 1st 2021 to January 31st 2023 A) average monthly**
487 **wind speed (m s⁻¹) and maximum wind gust, B) presented as a** wind rose diagram with wind speed and direction for
488 the period.

489

490

491

492

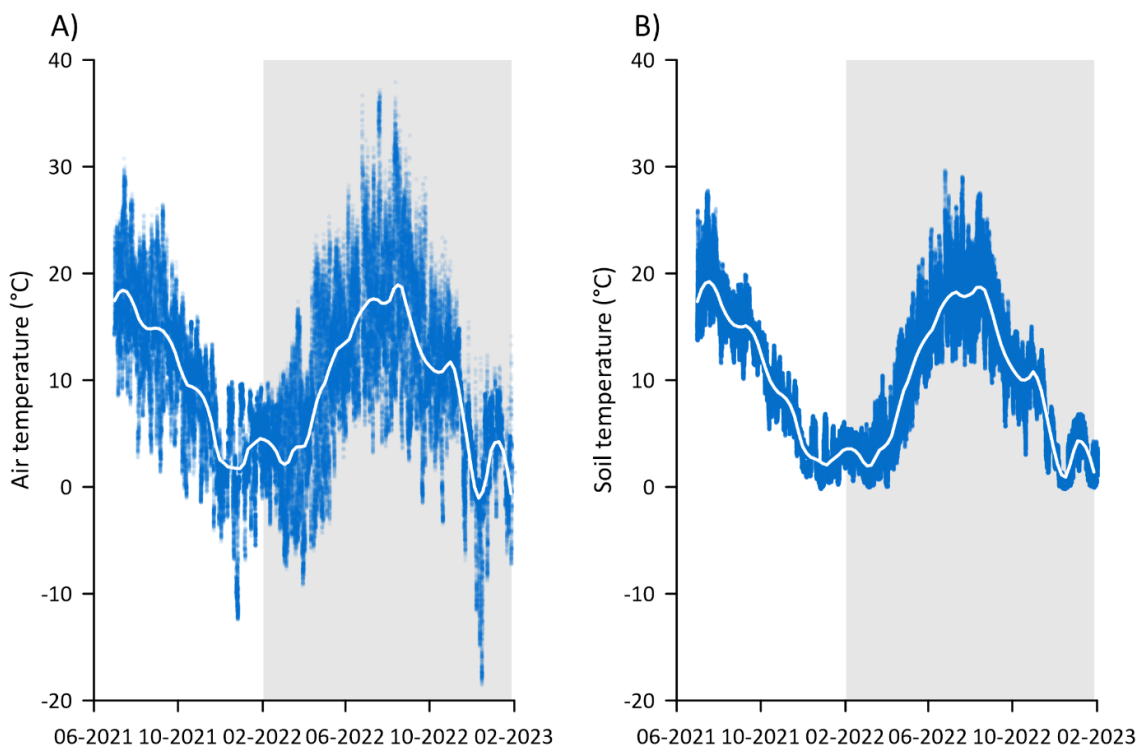
493

494

495

496

497



499

500 Figure 5: Time series of A) air temperature in °C measured at 2 meter height above the surface and B) soil
 501 temperature (°C) at 5 cm depth for collars 4, 7, 9, 23 and 27 along the measurement. The grey-blue dots are the raw 5
 502 min measurements of air temperature and the white blue lines represents are LOESS fit to show overall seasonal
 503 trend-daily means. The periods of GHG measurements with the SkyLine2D system are shown (green lines)with the
 504 shaded area on the x-axis.

505 The air temperature at Vejrumbro displayed typical seasonal variation for Danish conditions (Fig. 9). Over the
 506 study period the average air temperature was 9.6°C ranging between maximum 37.9°C and minimum of -18.6°C
 507 (Fig. 5A). Monthly ranges of air temperatures (Tab. 2) show >20°C variation between minimum and maximum,
 508 except for February, pointing towards large diurnal variations. Monthly mean, maximum and minimum
 509 temperatures shown in Table 2 show that the climate at Vejrumbro is quite dynamic with every month, except
 510 February, experiencing >20°C fluctuating between minimum and maximum temperatures pointing to large
 511 diurnal variations. Soil temperature magnitude and temporal variation were similar across the transect, varying
 512 between 0 to 28°C (Fig. 5B) and followed that of air temperature (Fig. 5A) with less variability (Fig. 5B and
 513 Table 3). The annual site average soil temperature was similar to the air temperature (Table 3).

514

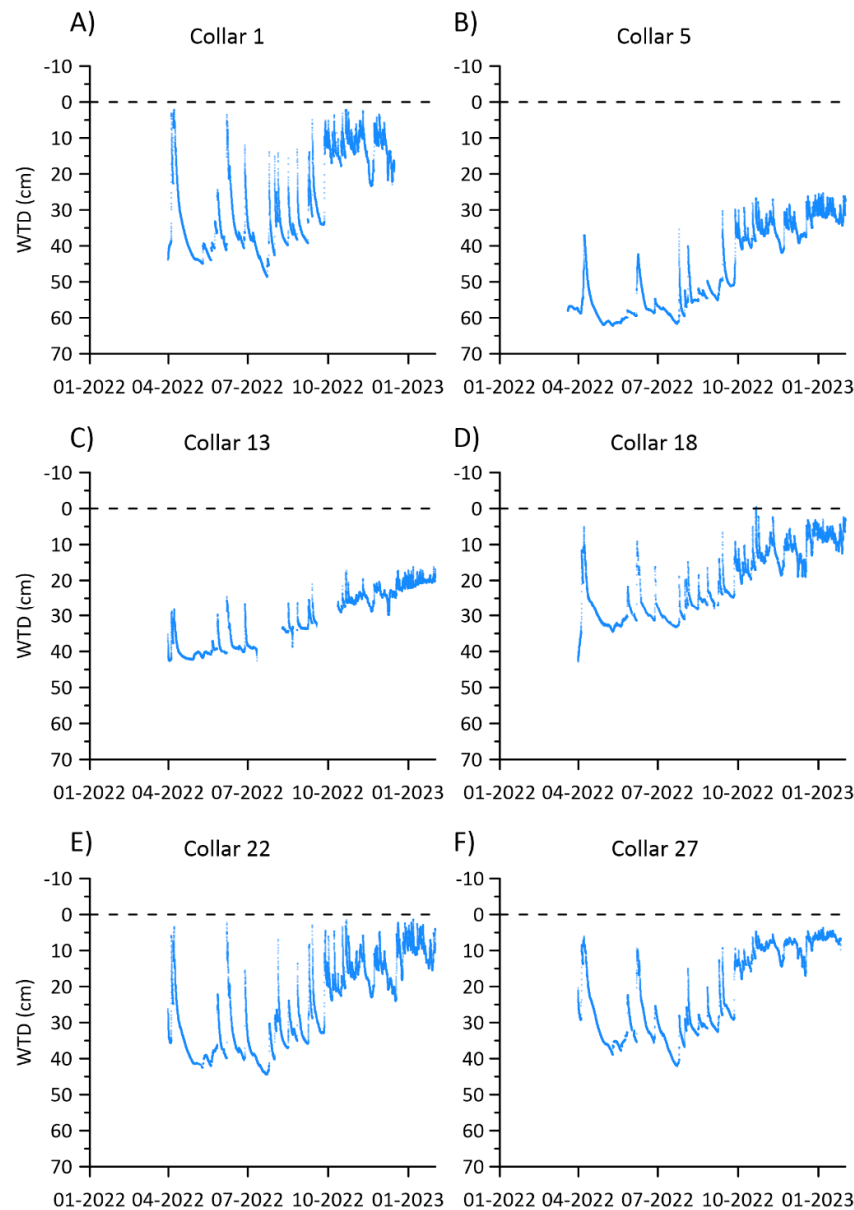
515 Table 322: Monthly mean, maximum and minimum air temperature and soil temperature (°C), groundwater table
 516 depth (cm) and volumetric soil water content (cm³ cm⁻³) at Vejrumbro in the measurement period from February 1st
 517 2022 to January 31st-2023.

Variable	Month	2022										2023		
		Feb	Mar	Apr	May	Jun	Jul	Aug	Sep	Oct	Nov	Dec	Jan	Avg
Air temperature (°C)	Mean	3.8	3.0	6.6	12.0	15.4	17.7	16.6	13.4	10.7	6.9	1.2	3.7	9.6
	Max	10.6	17.4	23.7	25.3	36.7	37.2	37.9	32.9	23.3	18.4	12.4	14.1	-
	Min	-4.3	-9.3	-8.3	-3.4	4.3	3.2	2.7	-1.5	-3.5	-6.9	-18.6	-7.3	-
Soil temperature (°C)	Mean	3.0	3.2	2.9	6.4	12.3	16.1	18.4	17.0	13.8	10.3	7.2	2.1	9.6
	Max	6.5	5.3	9.1	12.5	18.8	25.1	27.0	24.7	19.3	14.3	12.6	6.3	-
	Min	0.3	1.1	0.4	0.8	6.6	10.7	12.4	11.8	7.0	4.0	2.1	0.0	-
Groundwater table depth (cm)	Mean	-	39	35	41	36	41	35	31	20	18	17	13	29
	Max	-	58	39	58	43	52	46	36	30	31	28	28	-
	Min	-	23	5	24	9	28	22	9	5	6	3	2	-
Volumetric soil water content (cm ³ cm ⁻³)	Mean	0.53	0.45	0.40	0.37	0.38	0.43	0.43	0.45	0.50	0.53	0.52	0.51	0.46
	Max	0.56	0.51	0.50	0.41	0.47	0.55	0.56	0.56	0.57	0.58	0.56	0.57	-
	Min	0.43	0.39	0.37	0.33	0.32	0.26	0.32	0.35	0.40	0.47	0.42	0.34	-

518
 519

520 **3.4.3 Groundwater Water-table depth (WTD)**

521 Average groundwater table depth (WTD) below terrain during the period 47 to 21 cm across the
522 transect (Fig. 34, Table 23). During summer, the peat drained between 18 – 31 cm below the annual average and
523 in winter the WTD increased to 0 – 22 cm above the annual average across the transect (Fig. 43, Table 23).
524 Generally, the WTD was lower in the ditch across the entire study period (Fig. 43). It was only on the northern
525 end of the transect that the surface occasionally was flooded during winter periods (Fig. 34).



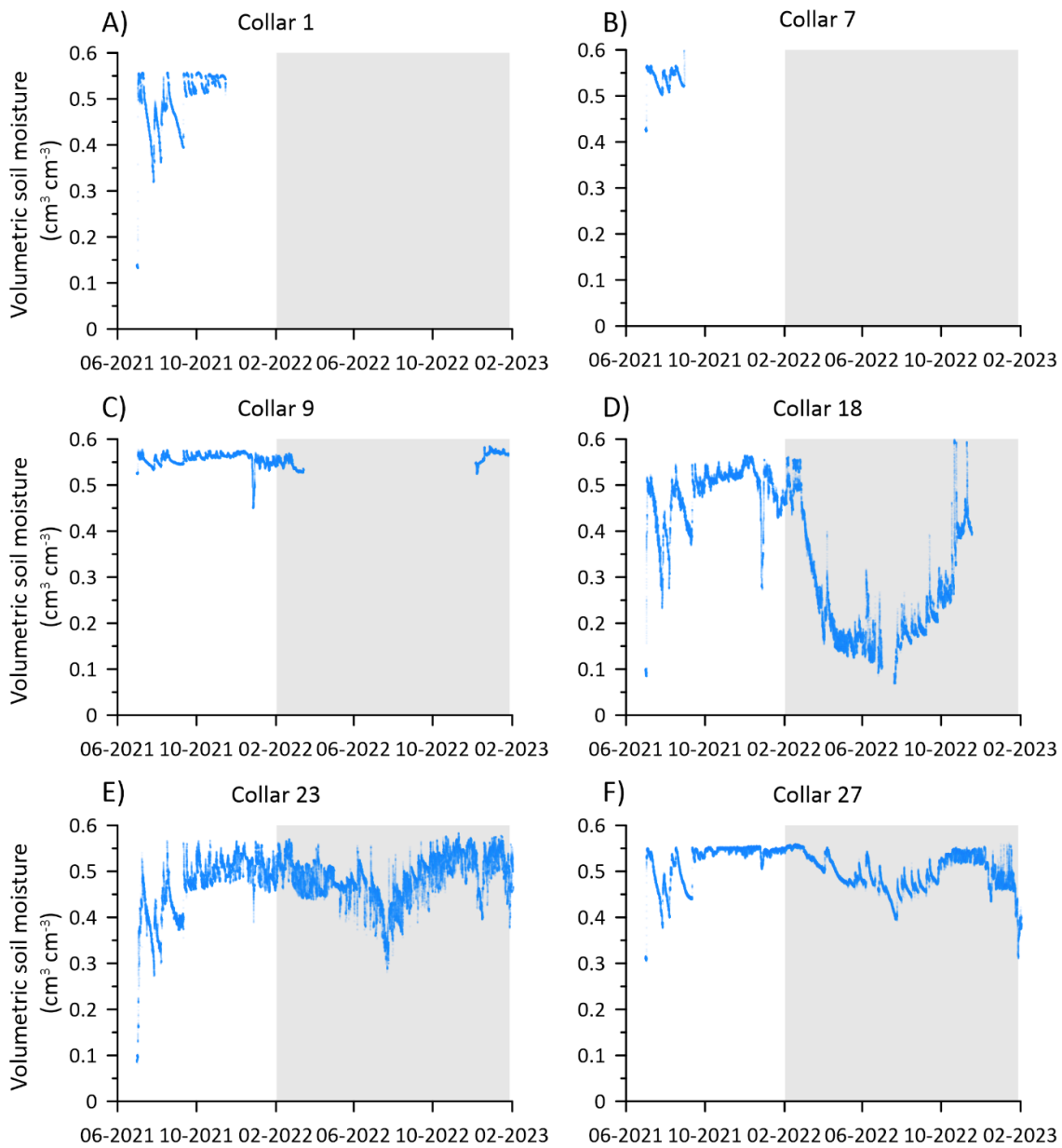
526
527 **Figure 614:** Time series of groundwater table depth (WTD) below terrain for the six piezometer locations along the
528 SkyLine2D transect in the period March 31st, 2022 and January 31st, 2023 – 31.01.2023 when the flux
529 measurements stopped. Dashed line show surface.

530 The temporal variability of Generally, the WTD displayed was similar across the transect similar temporal
531 variation despite different absolute water table depths (Fig. 11A-11F). In the summer periods, the WTD was

532 most variable decreasing to below -40 for collars 1, 13, 18, 22 and 27, whereas the WTD for collar 5 showed the
533 deepest groundwater measured at the site. WTD responded quickly (within hours) to precipitation events that
534 could increase the WTD by almost 40 cm at some plots, indicating that the entire aerated soil volume above the
535 groundwater table was flooded. There was a slight tendency to lower response to precipitation events for
536 piezometers at collar 5 and collar 13 that were placed closer to the ditch (Fig. 4-3 and 4-1B-6B and, C). As the
537 ditch water level was lower than in the peat this could be explained by more efficient lateral drainage into the
538 ditch from the areas closer to the ditch. In the winter periods, the WTD was less responsive to precipitation and
539 was closer to the surface (Fig. 4-1A-6A-F) across the transect.

540

541 3.5 Soil water content



542

543 Figure 742: Time series of volumetric soil water content ($\text{cm}^3 \text{cm}^{-3}$) in 0-5 cm for the six collars 1, 7, 9, 18, 23 and 27
 544 along the SkyLine2D transect in the period 01.07.2022–July 1st, 2021 – January 31st, 2023 when the
 545 measurements terminated. The periods of GHG measurements with the SkyLine2D system are shown (green lines) on
 546 the x-axis.

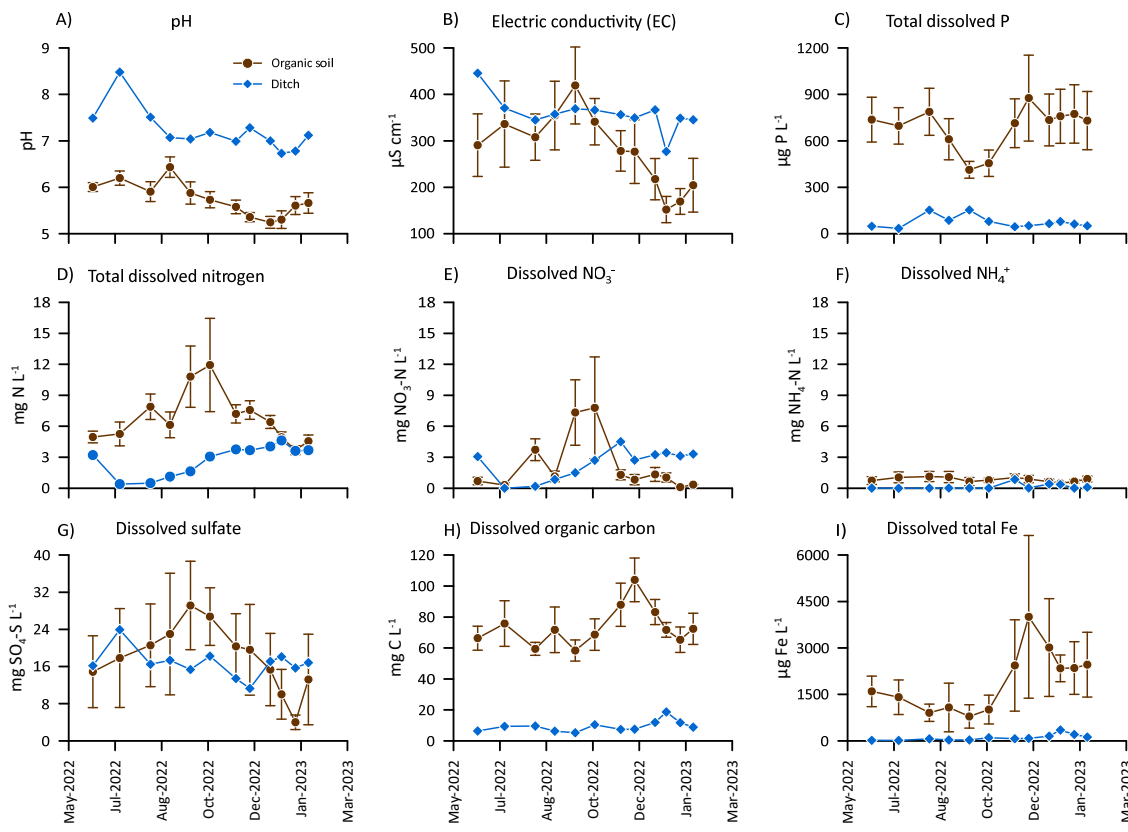
547 Due to instrument failure the temporal coverage of soil moisture in the top soil/topsoil (5 cm) was not similar
 548 across the transect (Fig. 12A-F). For collars 18, 23 and 27 the entire period of greenhouse gas measurements
 549 was covered by soil moisture measurements (Fig. 742D-F). While SWC for collars 1, 9, 18, 23 and 27 was
 550 similar in the winter periods (around $0.55 \text{ cm}^3 \text{cm}^{-3}$) the SWC for collar 18 decreased to lower minima between
 551 $0.1 - 0.2 \text{ cm}^3 \text{cm}^{-3}$, than the minima observed between $0.3 - 0.4 \text{ cm}^3 \text{cm}^{-3}$ for collars 23 and 27 in the summer
 552 periods (Fig. 127, Table 23). Similar for all collars it was observed that SWC was more variable in summer,

553 responding similarly as WTD to precipitation events (Fig. 427, Table 23). Since plants were removed regularly
554 from the collars the decrease of SWC for collar 18 cannot be explained by plant transpiration, and the dynamic
555 behaviour could indicate the impact of soil evaporation, but the different levels of SWC also show that there is
556 spatial variation across the transect in the drying properties of the soil. However, it cannot be ruled out that the
557 SWC sensor at collar 18 experienced malfunction or that soil contact was lost in the dry periods of 2022 (Fig.
558 12D7D) which could lead to erroneous and too low SWC. Therefore, these data should be considered with care.

559 3.6 Groundwater and ditch water chemical composition

560 Site mean pH of the groundwater in the organic soil was 5.8 ± 0.1 and was lower than the pH of the ditch
561 (7.3 ± 0.6). There was a tendency towards lower pH in groundwater and ditch towards the end of the
562 measurement period (Fig. ~~xxA8A~~). Electric conductivity was generally higher in the ditch water ($359 \pm 36 \mu\text{S}$
563 cm^{-1}) compared to the groundwater in the organic soil ($276 \pm 18 \mu\text{S cm}^{-1}$) ~~but~~ but varied less over the season.
564 The groundwater shows a clear peak in EC around September 2022 (Fig. ~~8xxB~~). Total dissolved P was
565 markedly higher in the groundwater ($687 \pm 45 \mu\text{g P L}^{-1}$) compared to the ditch water ($76 \pm 10 \mu\text{g P L}^{-1}$). Whereas
566 there was little seasonal trend in ditch P concentrations, dissolved P in groundwater dipped to below average
567 concentrations between August to October, likely indicating plant uptake during the growing season (Fig.
568 ~~8xxC~~). Similarly, total dissolved N was higher in groundwater ($6.7 \pm 0.5 \text{ mg N L}^{-1}$) than in ditch ($2.6 \pm 1.6 \text{ mg N}$
569 L^{-1}) with increasing concentrations during the growing season (Fig. ~~xxD8D~~). Similar, temporal trend was
570 observed for NO_3^- (Fig. ~~8xxE~~), but average groundwater ($2 \pm 0.5 \text{ mg NO}_3^- \text{N L}^{-1}$) and ditch ($2.2 \pm 1.5 \text{ mg NO}_3^- \text{N L}^{-1}$)
571 concentrations were similar. As ~~expected~~ expected, dissolved NH_4^+ -N was lowest among investigated N-
572 species and there was more dissolved NH_4^+ -N present in groundwater ($0.8 \pm 0.1 \text{ mg NH}_4^+ \text{N L}^{-1}$) than in the ditch
573 ($0.14 \pm 0.25 \text{ mg NH}_4^+ \text{N L}^{-1}$). However, there was no discernable temporal trend for NH_4^+ (Fig. ~~xx8F~~).
574 Collectively, the temporal trend of TN and NO_3^- could point to temperature driven mineralization of the peat.
575 Also, the organic N (TN – inorganic N-species) was on average 10 times higher in the groundwater than in the
576 ditch. Average SO_4^{2-} concentrations were similar between the groundwater ($17.5 \pm 2.4 \text{ mg SO}_4^- \text{S L}^{-1}$) and ditch
577 ($17 \pm 1.5 \text{ mg SO}_4^- \text{S L}^{-1}$), but SO_4^{2-} concentration peaked during September and October in the groundwater
578 whereas it remained more constant in the ditch over the season (Fig. ~~xx8G~~). Similar to dissolved organic N,
579 DOC concentrations were consistently higher in the groundwater ($73 \pm 3.1 \text{ mg DOC L}^{-1}$) than in the ditch
580 ($9.4 \pm 3.5 \text{ mg DOC L}^{-1}$), but peaked later in the season, around December 2022, whereas there was little temporal
581 variability of DOC in the ditch (Fig. ~~8xxH~~). Dissolved total Fe displayed the same temporal trend as DOC (Fig.
582 ~~8xxI~~) but was higher groundwater ($1916 \pm 163 \mu\text{g Fe L}^{-1}$) compared to the ditch ($98 \pm 95 \mu\text{g Fe L}^{-1}$). The
583 geochemical parameters of groundwater and ditch water point to different mechanisms regulating especially
584 elements related to peat decomposition and possibly plant uptake, where groundwater was more dynamic over
585 time than ditch water. Generally, there were no systematic spatial pattern of groundwater chemistry across the
586 transect.

587



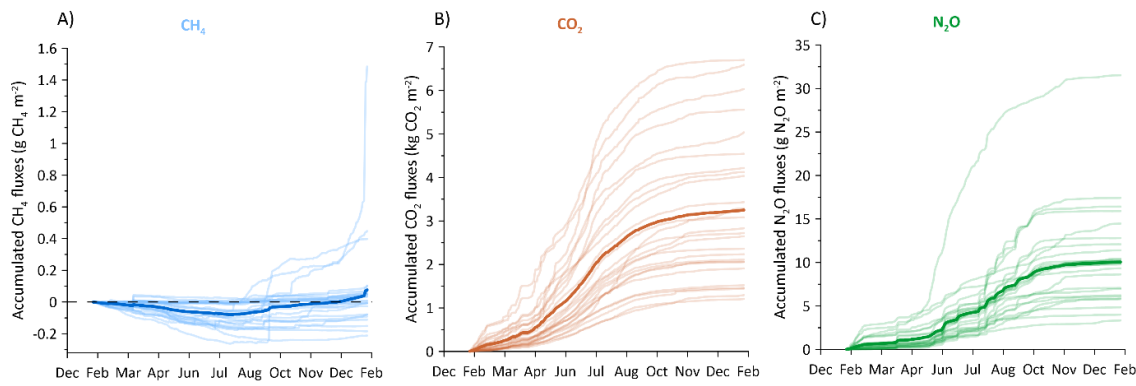
588
589
590
591
592
Figure 82 Groundwater (brown closed circles) and ditch water (closed blue diamonds) chemistry at Vejrumbro for
the period June 2022 to February 2023 for A) pH, B) Electric conductivity and dissolved C) total phosphor (P), D)
total nitrogen (N), E) nitrate (NO_3^-), F) ammonium (NH_4^+), G) sulfate (SO_4^{2-}), H) organic carbon and I) total iron
(Fe). Values for organic soils are site means with error bars showing the standard error of the mean (N=6 per
sampling date).

593

594 3.6-7 Net soil and ditch CO_2 , CH_4 and N_2O fluxes

595 3.6.7.1 Spatial variation of net soil CO_2 , CH_4 and N_2O fluxes

596



597
598
599
Figure 9813: Cumulative fluxes of A) CH_4 , B) CO_2 , and C) N_2O for 26 individual collars along the SkyLine2D
transect. Units for CH_4 and N_2O are in $\text{g CH}_4/\text{N}_2\text{O m}^{-2}$ and for CO_2 in $\text{kg CO}_2 \text{m}^{-2}$. The cumulative fluxes represent
the raw dataset. The ditch data was excluded. Site average is shown as thick lines.

600 Within the transect, cumulative CH₄ fluxes over the study period (360 days) varied between -0.21 to 1.48 g CH₄
601 m⁻² over the study period, with a site average (\pm SE) cumulative flux of 0.07 \pm 0.06 g CH₄ m⁻² (Fig. 43A-3 and
602 9A and 14). Out of the 26 collars, excluding the ditch collar, 11 displayed a net uptake over the measurement
603 period and the remaining were small net emitters (Fig. 43A and 149A). There was generally little spatial
604 variation in the absolute CH₄ fluxes among the soil collars, but three collars (11, 12 and 15) showed increasing
605 net positive cumulative fluxes towards the ditch (Fig. 143). The low spatial and similar temporal variation
606 between collars indicate both hydrological indicators of SWC and WTD are poor predictors of CH₄ fluxes at this
607 site. However, as we excluded plants from the collars we might have decreased the net emission of CH₄ directly
608 by restricting gas transport in aerenchyma (Askaer et al. 2011; Vroom et al. 2022) and indirectly by potentially
609 reducing plant carbon supply to methanogens. However, visible inspection at the site confirmed lateral root
610 growth from vegetation adjacent to the collar. This could indicate that plant derived C and N was still available
611 for microbes underneath the collars, but the impact on gas transport is uncertain. However, we did not excavate
612 roots during the study to avoid excessive disturbance. Furthermore, considering that the WTD in the growing
613 season was mostly 20-40 cm below terrain the potential for CH₄ production in the topsoil would limited (Koch
614 et al. 2023). Also, the lack of consistent hot moments of CH₄ emissions and low cumulative emissions from the
615 soil despite hydrological conditions in the subsoil being conducive for CH₄ production could indicate that redox
616 potential is elevated due to presence of other electron acceptors. The presence of both free NO₃⁻, SO₄²⁻, Fe (Fig.
617 8E, G, I) in the groundwater could indicate that there are alternative electron acceptors that prevent lowering of
618 the redox status of the soil and hence suppresses CH₄ production.

619 The CO₂ effluxes displayed tremendous spatial variation across the 24-meter transect (Fig. 3 and 913B and 14) and measurements indicated that the drained peat organic soil was a net source of CO₂, with cumulative fluxes over the study period ranging between 1214 – 6740 g CO₂ m⁻², and a site average (\pm SE) of 3269 \pm 328 g CO₂ m⁻², over the study period of 360 days (Fig. 3 and 943B and 14). There was no apparent relation between the magnitude of cumulative CO₂ efflux to the position along the transect and average WTD (Fig. 143). The cumulative net soil CO₂ emission is equal to 8.9 tCO₂-C ha⁻¹ y⁻¹ (range of 3.3 to 18 tCO₂-C ha⁻¹ y⁻¹ across the transect) and compares well to estimates of annual soil C loss (8.8 tCO₂-C ha⁻¹ y⁻¹) from a drained unfertilized grassland on organic soil in Denmark (Kandel et al. 2018) as well as annual carbon budgets of similar Danish, British and German wetlands (Tiemeyer et al. 2020; Evans et al. 2021; Koch et al. 2023).

628 Similarly, the site was overall a net source of N₂O, with cumulative fluxes ranging between 3.3 – 32 g N₂O m⁻², with a site average (\pm SE) of 10.1 \pm 1.1 g N₂O m⁻² (Fig. 3 and 943C) over the study period (360 days). Thus, there is a 10-fold difference between minimum and maximum cumulative N₂O fluxes within the transect, without any apparent relation to the position along the transect and WTD. The highest cumulative N₂O fluxes occurred at collar 8 situated close to the ditch (Fig. 143).

633 The site average cumulative N₂O emission is equivalent to a net N loss from N₂O emission alone of 64 kg N ha⁻¹ y⁻¹, was very high and exceeding previously reported fluxes from this site (1.5 – 2.1 g N₂O m⁻² y⁻¹) (Nielsen et al., 2024) and German organic soils (0.04 – 6.3 g N₂O m⁻² y⁻¹ for grassland and cropland land uses) (Tiemeyer et al. 2020). The high N₂O emission from this site during the measurement period indicate that N₂O may in fact dominate the GWP budget at this site had gross primary production been included in the measurements. It is

638 important to reiterate here that the flux measurements of this study were done on bare soil whereas the studies
639 referenced above included vegetation.

640 The high N₂O fluxes may be a result of high rates of denitrification in the subsoil from either *in situ* produced
641 NO₃⁻ from peat decomposition or as NO₃⁻-enriched agricultural runoff from the surrounding intensively
642 cultivated areas, which was not affecting groundwater NO₃⁻ concentration in the center of the wetland with
643 lower N₂O (Nielsen et al. 2024). The groundwater enters the northern peripheral zone of the wetland at
644 Vejrumbro coinciding with the position of the measurement transect. The highest NO₃⁻ concentrations in
645 groundwater at the SkyLine2D transect corresponded roughly with highest N₂O emission during summer and
646 early autumn (Fig. 8D-F and Fig. 12D), but the frequency of water sampling was too low to fully link
647 groundwater NO₃⁻ temporal dynamics to N₂O emissions.

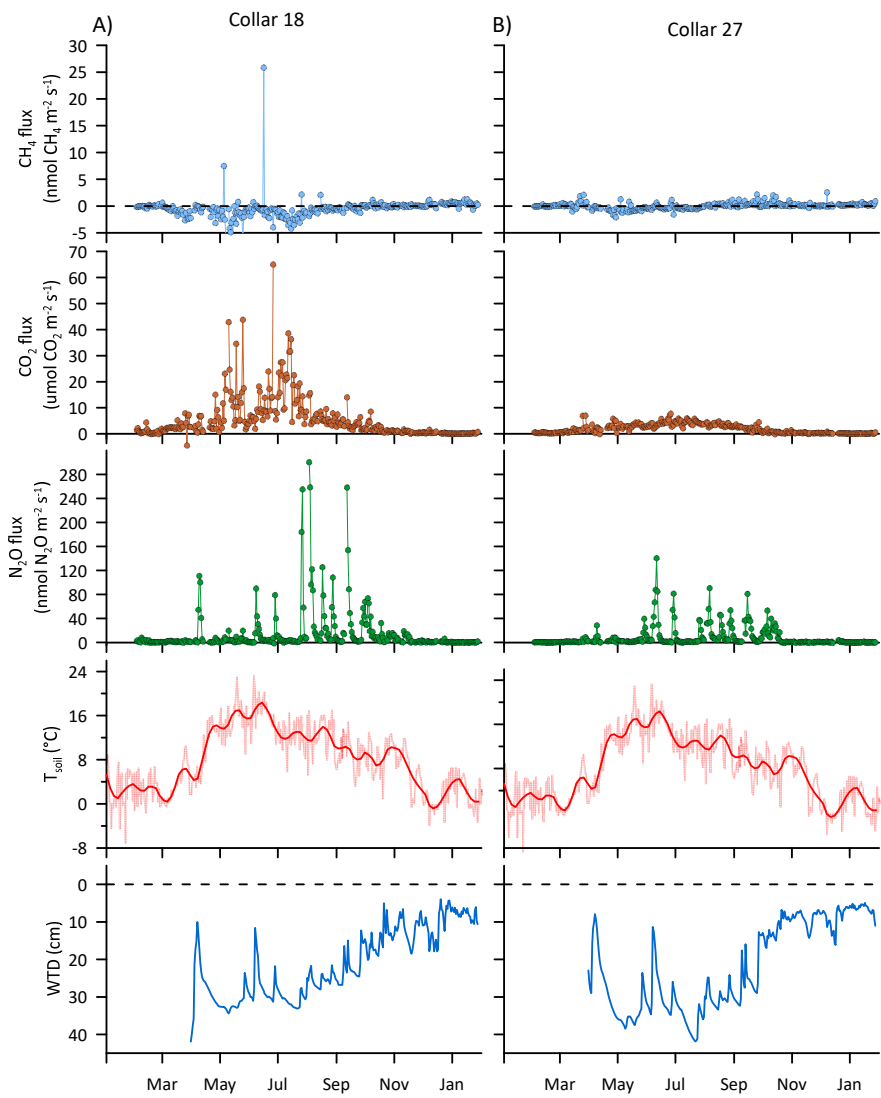
648

649 **Figure 14: The annual cumulative fluxes of CO₂ (red) (kg CO₂·m⁻²·y⁻¹), N₂O (green) (g N₂O·m⁻²·y⁻¹) and CH₄ (blue) (g**
650 **CH₄·m⁻²·y⁻¹) over the measurement transect at Vejrumbro. Closed and open symbols for CH₄ represent net**
651 **cumulative emission and uptake, respectively.**

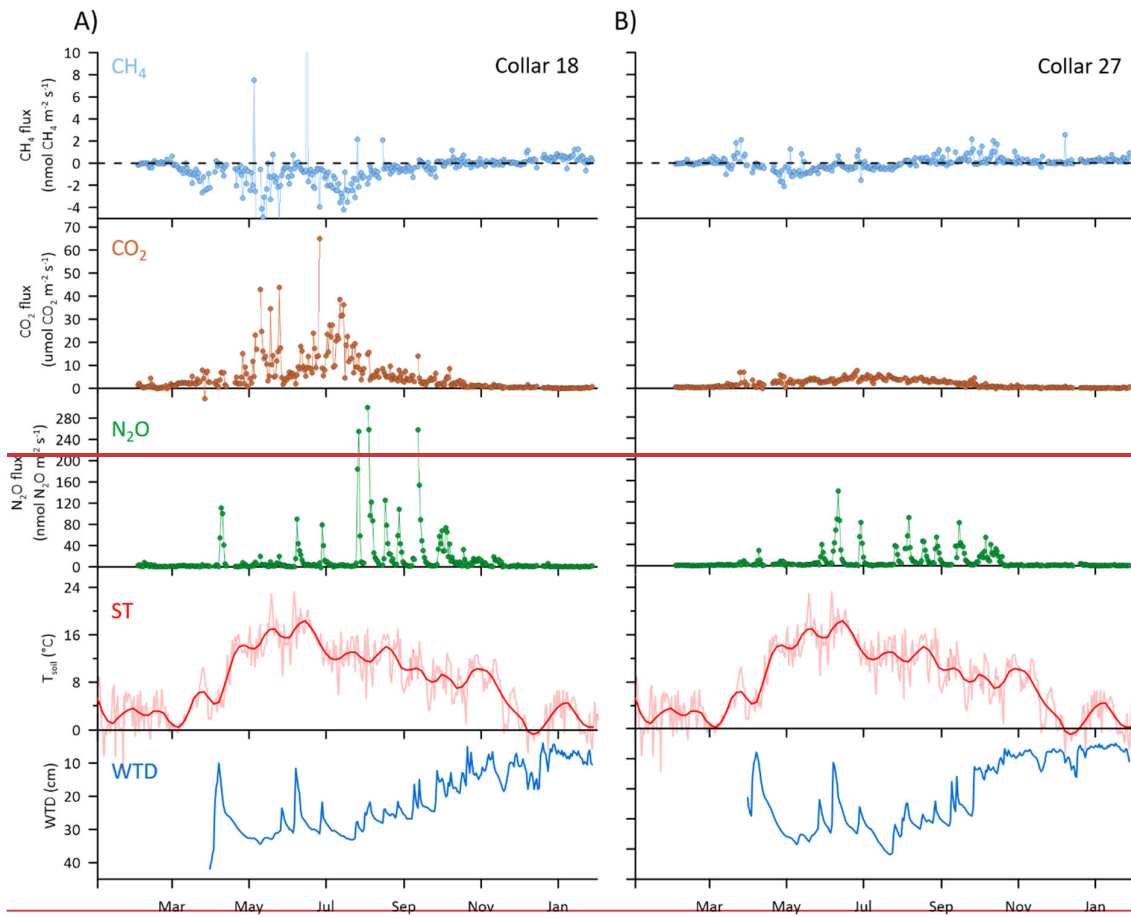
652

653 3.67.2 Temporal variability of net soil CO₂, CH₄ and N₂O fluxes

654 3.67.2.1 Time series of raw data of net soil CO₂, CH₄ and N₂O fluxes



655



656
657 **Figure 10915:** Examples of daily average time series of CH₄, CO₂ and N₂O fluxes for collars 18 and 27 at the
658 SkyLine2D transect in Vejrumbro. Soil temperature (ST) in celsius (°C) and groundwater table depth (WTD) in cm
659 below terrain is shown in two lower panels.

660 With the high frequency of GHG flux measurements (on average 5 measurements per day per collar) it was
661 possible to observe short term flux phenomena that in most studies deploying manual chambers are missed or if
662 captured can lead to biased conclusions on flux magnitudes. For example, in most of the measurement points,
663 CH₄ fluxes were generally near zero, but occasionally displayed elevated net emission for short periods even in
664 periods with deeper WTD (Fig. 15A10A) for most chambers (see supplementary Fig. S4S5). This flux dynamic
665 might be related to episodic release of accumulated CH₄ from deeper soil layers that are not fully oxidized in the
666 aerated root zone and that were not released through plants (Askaer et al. 2011). As plants were not included in
667 the collars these bursts cannot be attributed to plant emission pathways. Click or tap here to enter text.

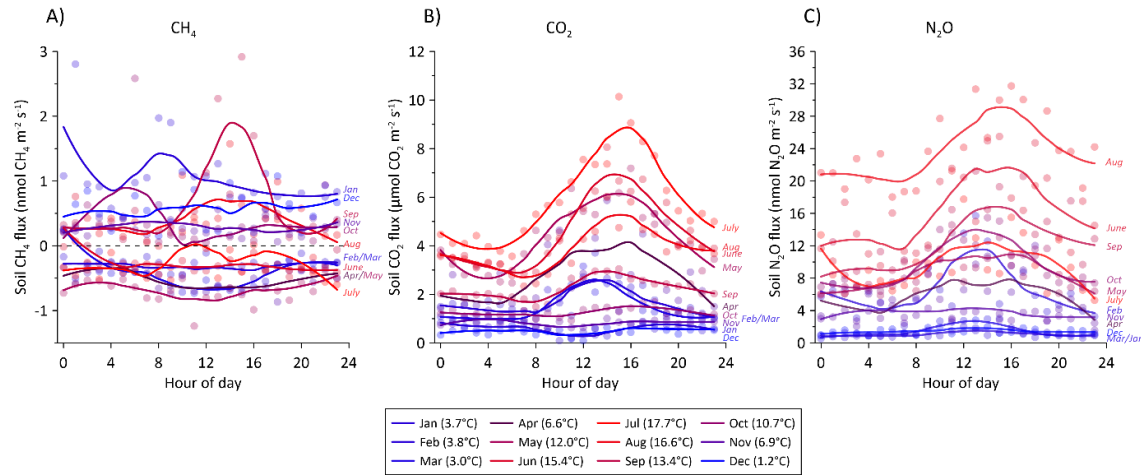
668 For net soil CO₂ fluxes the short term flux dynamics differed between chambers (Fig. 15A and B). Generally,
669 Often it was observed that soil CO₂ fluxes would show an increased over the season with increasing temperature.
670 However, for some collars displayed seasonally increasing flux superimposed by rapid, within hours, bursts of
671 CO₂ emissions (example in Fig. 15A10A), while other collars at the same period did not display this behaviour
672 (Fig. 15B10B). This dynamic points to different emission pathways from the soil not related to plant mediated
673 transport. Thus, while we purposely omitted aboveground autotrophic respiration by clipping the vegetation, it

674 cannot be ruled out that living roots inhabited the soil below the chambers and hence contributed to the observed
675 CO₂ emission rates.

676 For N₂O, the spatiotemporal pattern was even more pronounced than for CO₂, with N₂O primarily generally
677 across the transect being emitted in bursts related to rapidly increasing or decreasing WTD that coincided with
678 precipitation events. In drier periods with deeper WTD and little fluctuations, N₂O fluxes quickly dropped to
679 near zero (Fig. 15A-10A and B). Despite N₂O being emitted in similar temporal patterns across the site, the
680 magnitude of the N₂O peaks were not similar across the transect (Fig. 15-10 and supplementary Fig. S+S5).
681 Hence, the majority of N₂O is emitted in hot moments driven by fluctuations in WTD mainly (Fig. 15-10) as it
682 has also been shown in other drained temperate peatland soils (Anthony and Silver 2023). In a dry forest
683 ecosystem similar temporal patterns of N₂O fluxes have been found, but albeit driven by different soil
684 physicochemical mechanism.

685

686 33.67.2.2 Diurnal variation of net soil CO₂, CH₄ and N₂O fluxes



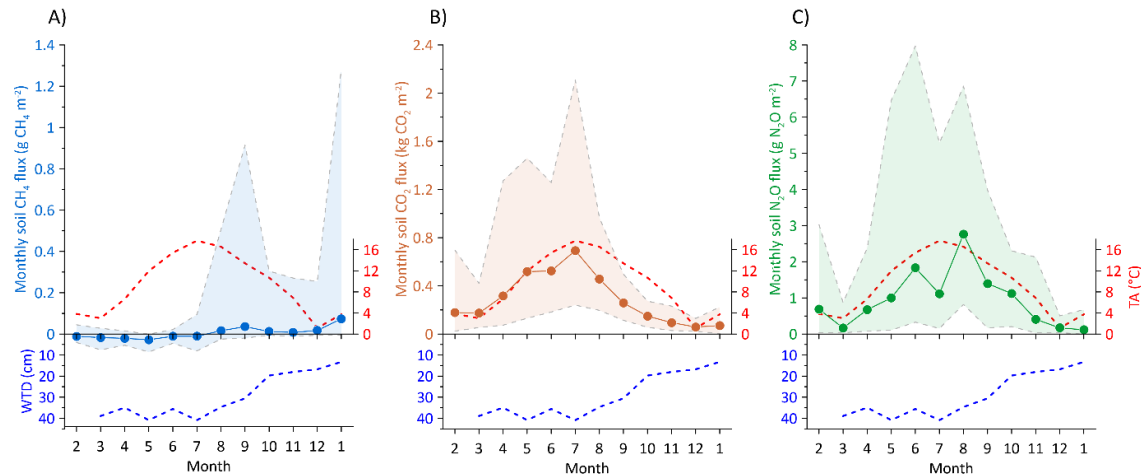
687

688 Figure 111016: Average hourly flux for all soil collars of A) CH₄, B) CO₂, and C) N₂O during a 24 hour period. The diurnal variation is split between each month during the 2022-2023 measurement period. The fluxes were assigned the hour of measurement during the day and averaged per month. Color shade between blue and red corresponds to average monthly air temperature for the specific month shown in parenthesis in the figure legend. Solid lines are loess fits for visualization of the diurnal variation in each month.

693 With the SkyLine2D system we observed a clear diurnal variation cycle for CO₂ and N₂O fluxes, but not for
694 CH₄ (Fig. 16A-11A-C). The lack of diurnal variability of CH₄ fluxes could also be due the removal of plants
695 from the collars that would have facilitated light-driven fluxes (Askaer et al. 2011). The amplitude of diurnal
696 variability increased with higher air temperature for CO₂ (Fig. 16B) and partly for N₂O (Fig. 16C). The with
697 the month of July was an exception as it resembled the pattern observed in May although the July soil
698 temperature was about 5°C higher in July than in May (Table 2). The lower N₂O fluxes observed in July can be
699 attributed to lower and more constant WTD in July compared to May, June and September across the transect
700 (Fig. 64). Diurnal variability of soil CO₂ fluxes are well known and can be related to both increased

701 heterotrophic respiration during the warmer day and autotrophic respiration in response to photosynthesis.
702 Previously, similar diurnal patterns of N_2O emissions were observed in a Danish fen (Jørgensen et al. 2012).

703 **3.6.7.2.3 Monthly variability of net soil GHG fluxes**



704
705 **Figure 121117:** Monthly summed soil fluxes of A) CH_4 in $\text{g CH}_4 \text{ m}^{-2}$, B) CO_2 in $\text{kg CO}_2 \text{ m}^{-2}$, and C) N_2O in $\text{g N}_2\text{O m}^{-2}$
706 for all organic soil collars. Shaded areas for CH_4 , CO_2 and N_2O graphs represent the maximum and minimum
707 monthly average fluxes. Blue dashed line below CH_4 , CO_2 and N_2O represent the measured monthly average transect
708 groundwater table depth (WTD) in cm below terrain. Red dashed line shows the monthly average air temperature
709 (TA).

710 The average soil GHG fluxes for all collars were summed to monthly transect average site sums to illustrate
711 long term drivers on the flux magnitude. Overall, monthly sums of CO_2 and N_2O emissions fluxes relate both
712 to increase with temperature increase and fluxes are highest under deeper WTD, but CH_4 net fluxes were less
713 responsive to long term changes in both temperature and hydrology lowering of the ground water table (Fig.
714 1712A-C). The lowest seasonal response was observed for CH_4 (Fig. 17A) where the flux was generally around
715 zero. Net uptake increased slightly with increasing temperature and lower WTD during the spring and summer.
716 With increasing water table and high temperatures in August the site turned into a small net CH_4 source
717 continuing in fall and winter (Fig. 17A12A).

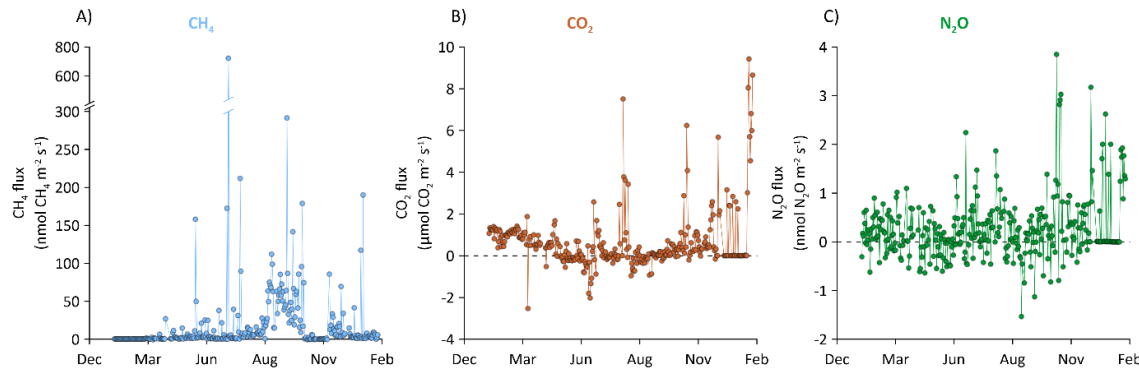
718 For CO_2 the seasonal variation was pronounced and closely followed soil temperature until peak values in July
719 for both site average, minimum and maximum fluxes, respectively (Fig. 17B). From July to August, it
720 was observed that WTD at the site began to increase again and CO_2 fluxes departed from the close relation to
721 soil temperature, indicating an inhibitory role of the WTD in this period, but reaching minimum fluxes in
722 December, corresponding to the wettest and coldest month (Fig. 17B12B).

723 Similarly, N_2O fluxes increased with soil temperature reaching peak monthly values in August, corresponding to
724 the period of the year with highest soil temperature and increasing WTD (Fig. 17C). This supports the
725 promoting role of soil water saturation on the production of N_2O when temperature is favourable for
726 denitrification. N_2O fluxes reached minimum values in December when WTD and ST were lowest (Fig. 17C).

728

729 **3.67.3 Ditch CO₂, CH₄ and N₂O fluxes**730 **3.67.3.1 Time series of raw data of ditch CO₂, CH₄ and N₂O fluxes**

731

732
733 **Figure 13418: Daily average time series of net ditch total A) CH₄ (diffusion and ebullition), B) CO₂, and C) N₂O**
734 **fluxes at the Vejrumbro site.**

735 Common for all three gases is that ditch emissions are dynamic and net fluxes change from zero to large net
 736 positive or negative fluxes within hours or days (Fig. 138A-C). Compared to net soil CH₄ fluxes the ditch can be
 737 considered an emission hotspot at the site (sum of diffusive and ebullition: 8.3 g CH₄ m⁻² y⁻¹), but fluxes are
 738 lower than earlier reports for ditches in other drained wetlands (between 0.1 – 44.3 g CH₄ m⁻² y⁻¹) (Peacock et
 739 al., 2021). Methane is most dynamic with maximum diffusive flux close to 700 nmol CH₄ m⁻² s⁻¹ and there
 740 was a tendency toward consistently higher net CH₄ emission from August to September, becoming close to zero
 741 in colder seasons (Fig. 138A). Ebullition of CH₄ did occur occasionally in the ditch, e.g. about 19.3% of flux
 742 measurements for the ditch was comprised of ebullitions but constituted on average only 2.9% of the total CH₄
 743 emission (0.24 g CH₄ m⁻² y⁻¹) from the ditch which is lower, but in the same range as a recent estimate from a
 744 ditch in a similar drained German peatland (Köhn et al. 2021). but a According to the flux calculation
 745 methodology and flux separation and extrapolation to daily sums, diffusive fluxes dominated (6.56 g CH₄ m⁻²
 746 y⁻¹). However, it cannot be ruled out that the classification as diffusive flux may in fact be ebullition by nature.
 747 It has been suggested that microbubbles resulting from mass transport can resemble diffusive fluxes in a
 748 chamber making it difficult, if not impossible, to fully separate the two emission mechanisms in a continuous
 749 time series if headspace CH₄ concentrations do not abruptly increase (Prairie and del Giorgio 2013), such as in
 750 the example shown in Fig. 7S4. Hence, here the CH₄ fluxes are represented as total CH₄ flux, i.e. the sum of
 751 diffusive and ebullition. Compared to net soil CH₄ fluxes the ditch can be considered an emission hotspot at the
 752 site (10.4 g CH₄ m⁻² y⁻¹), but fluxes are lower than earlier reports for ditches in other drained wetlands (between
 753 0.1 – 44.3 g CH₄ m⁻² y⁻¹)

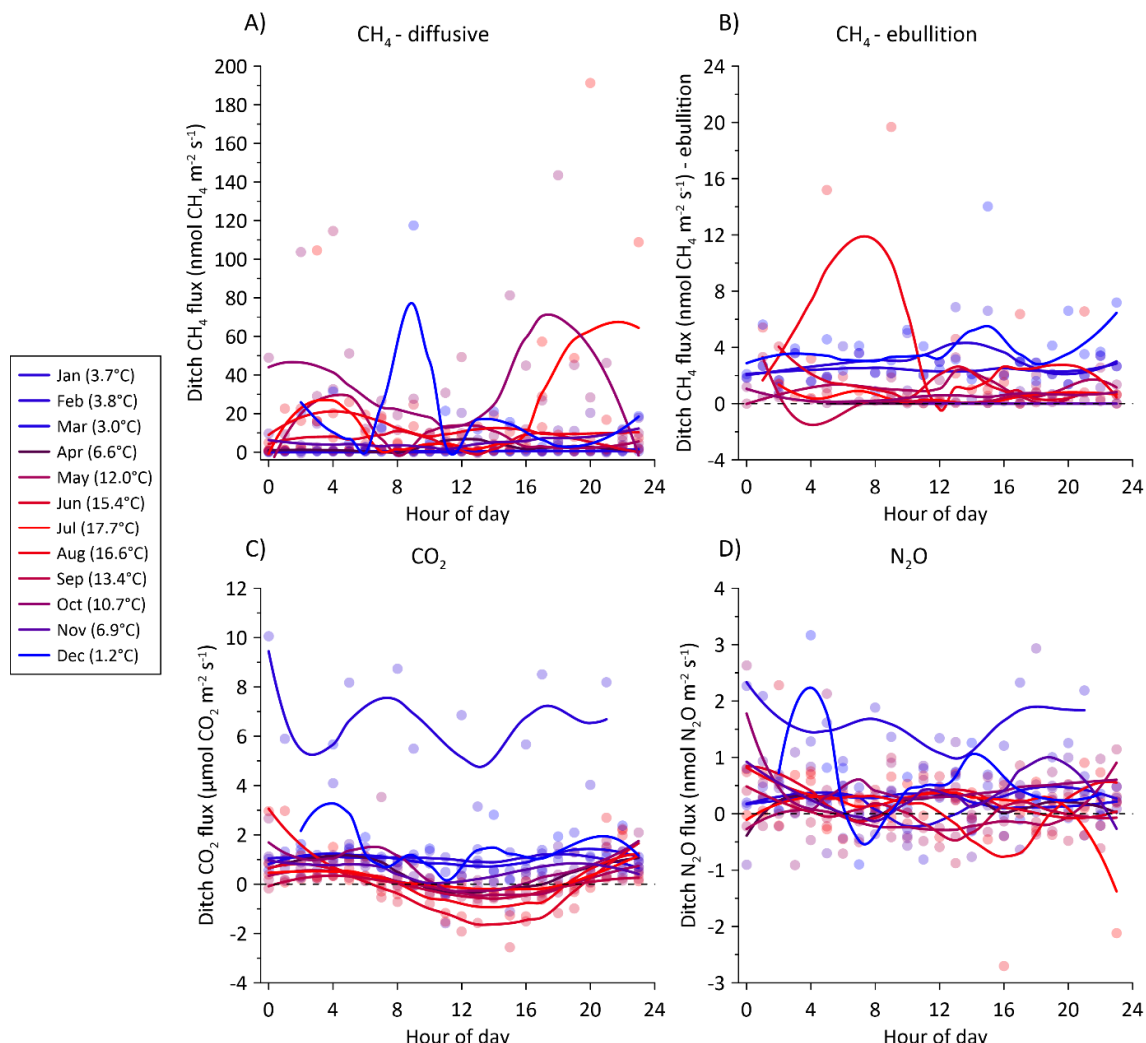
754 For CO₂, there was a general tendency towards lower fluxes during the summer months and fluxes increased in
 755 magnitude and variability towards the end of the study period (Fig. 183B). For N₂O, the fluxes fluctuated
 756 around zero for most of the study period, except towards the end (December and January) where net fluxes
 757 became positive (Fig. 48C13C).

758 Compared to the net soil N₂O and CO₂ fluxes the ditch fluxes of these gases are low showing that the ditch is
759 not contributing significantly to the CO₂ and N₂O budget at this site.

760

761 Per square meter, the ditch emitted less N₂O (0.41 g N₂O m⁻² or 2.6 kg N₂O-N ha⁻¹ y⁻¹) and CO₂ (961 g CO₂ m⁻²
762 y⁻¹ or 2.6 tCO₂-C ha⁻¹ y⁻¹) than the organic soil, but was a hotspot of CH₄ emission (8.4 g CH₄ m⁻² y⁻¹ or 63 kg
763 CH₄-C ha⁻¹ y⁻¹) during the measurement period. Although these emissions estimates are lower than previously
764 reported for ditches in organic soil (up to 44 g CH₄ m⁻² y⁻¹) (Peacock et al. 2021). For the ditch CH₄ budget,
765 ebullition only constitutes 2.9% of net CH₄ emissions during the study period. This proportion may be
766 underestimated as the count of ebullition events may have been underestimated (Prairie and del Giorgio 2013).

767

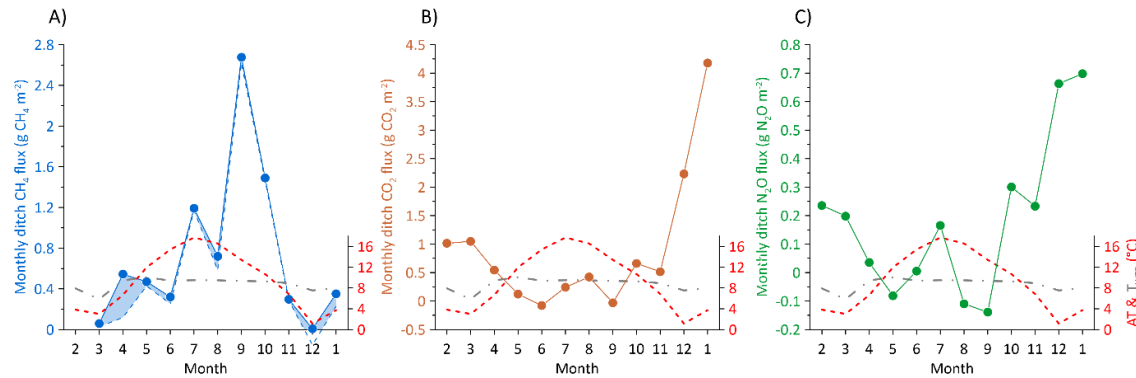


770 Figure 141319: Average hourly flux for A) CH_4 -diffusive fluxes, B) CH_4 -ebullition fluxes, C) CO_2 , and D) N_2O during
 771 24 hours from the ditch. Colours correspond to average monthly air temperature shown in parenthesis in the figure
 772 legend. Note different axes. Average hourly fluxes for the ditch collar of A) diffusive CH_4 fluxes, B) CH_4 ebullition
 773 fluxes, C) CO_2 , and C) N_2O during a 24 hour period. The fluxes were assigned the hour of measurement during the
 774 day and averaged per month. The diurnal variation is split between each month during the 2022-2023 measurement
 775 period. Color shade between blue and red corresponds to average air temperature for the specific month shown in
 776 parenthesis in the figure legend. Solid lines are loess fits for visualization of the diurnal variation in each month. Note
 777 different axes.

778 For CH_4 fluxes, both diffusive and ebullition, there was no clear diurnal variability in any month (Fig. 194A and
 779 B). This is expected for ebullition emissions which is known to be erratic without any clear diurnality (Wik et al.
 780 2016; Sø et al. 2023). For net CO_2 fluxes from the ditch there was no diurnal variability in colder seasons (Jan,
 781 Feb, Mar, Nov and Dec), but consistent positive net CO_2 efflux (Fig. 194C). Diurnal patterns became more
 782 clearer with higher temperatures from May to October (Fig. 149C) and in this period CO_2 fluxes decreased
 783 during the day to sometimes reach net negative fluxes (net uptake of CO_2) during and after midday (Fig. 194C),

784 although the net emissions were also observed in the daytime period (Fig. 194C). The net negative fluxes can
 785 likely be explained by photosynthetic activity of aquatic plants on the surface of the ditch or by algae in the
 786 water column which was measured due to the transparency of the chamber. Using an opaque chamber instead
 787 would likely have resulted in different net CO₂ efflux in daytime. For N₂O, the same pattern as for CH₄ was
 788 observed, where flux magnitude across the day fluctuated around zero, except for January where N₂O fluxes
 789 were consistently above zero (Fig. 14D)-(Fig. 19D).

790 3.67.3.3 Monthly variability in ditch fluxes



791 **Figure 151420:** Monthly summed ditch fluxes of A) CH₄ in g CH₄ m⁻², B) CO₂ in g CO₂ m⁻² and C) N₂O in g N₂O m⁻².
 792 In A) the blue dashed line is the contribution of diffusive fluxes and the shaded blue area between the full and dashed
 793 blue lines represent the monthly contribution of ebullition to the total flux. Red and grey dashed lines show the
 794 monthly average air (AT) and groundwater temperature (Twrd) in °C, respectively.
 795

796 The monthly sums of CH₄ tend to increase show proportionality to with air temperature, although peak CH₄
 797 emissions (September) occurred after air temperature peak (July) (Fig. 20A15A). Diffusive fluxes comprised the
 798 major emission pathway of CH₄ in the ditch (between 21% - 99%), with the contribution from ebullition being
 799 highest in March (55%) and April (78%) (Fig. 20A15A). Water temperature in the ditch was relatively stable
 800 throughout the year, varying between 5.8 – 10.1°C being highest from April to November and lowest from
 801 December to March. However, there is little indication of a direct relation between ditch water temperature and
 802 net GHG fluxes (Fig. 2015A-C).

803 For CO₂ and N₂O, the seasonal pattern is reversed with lowest fluxes during the warmest periods, approaching
 804 net zero or even net negative fluxes (Fig. 2015B and C).

805 3.67.4 Estimate of the annual soil and ditch GHG budgets at the Vejrumbro location

806 The annual GHG flux data was summarized to annual budgets for N₂O, CO₂ and CH₄ were adjusted from the
 807 cumulated values by multiplying with a factor of 365/360. It (Table 3) showed ing that for the drained peat
 808 organic soil its gaseous carbon loss was mostly as CO₂, while CH₄ played a negligible role in the C cycle and
 809 consequently also for global warming potential (GWP) budget. The annual soil CO₂ loss of 3,632 g CO₂ m⁻² y⁻¹
 810 is equal to 9.9 tCO₂ C ha⁻¹ y⁻¹, which compares well to an estimate of annual soil C loss (8.8 tCO₂ C ha⁻¹ y⁻¹)
 811 from a drained unfertilized grassland on organic soils in Denmark (Kandel et al. 2018) as well as annual carbon
 812 budgets of similar Danish, British and German wetlands (Tiemeyer et al. 2020; Evans et al. 2021; Koch et al.

813 Annual N_2O emissions were very high (site average: $10.4 \text{ g N}_2\text{O m}^{-2} \text{ y}^{-1}$ ranging at this site exceeding
 814 previously reported fluxes from this site (Nielsen et al., 2024) and German organic soils (0.04 – $6.3 \text{ g N}_2\text{O m}^{-2} \text{ y}^{-1}$
 815 ⁴ for grassland and cropland land uses) (Tiemeyer et al. 2020). The annual N_2O GWP contribution is 47%
 816 compared to 53% for CO_2 , indicating that N_2O may in fact dominate the GWP budget at this site had gross
 817 primary production been included in the measurements. It is important to reiterate here that the flux
 818 measurements of this study were done on bare soil whereas the studies referenced above included vegetation.
 819 Thus, while we purposely omitted aboveground autotrophic respiration, it cannot be ruled out that living roots
 820 inhabited the soil below the chambers and hence contributed to the observed CO_2 emission rates.

821 The high N_2O fluxes may be a result of high rates of denitrification in the subsoil as NO_3^- -enriched agricultural
 822 runoff from the surrounding intensively cultivated areas, which was not affecting groundwater NO_3^-
 823 concentration in the center of the wetland with lower N_2O (Nielsen et al. 2024). The groundwater enters the
 824 northern peripheral zone of the wetland at Vejrumbro coinciding with the position of the measurement transect.
 825 Although, sporadic measurements of NO_3^- concentrations in groundwater at the SkyLine2D transect did show
 826 elevated NO_3^- , it may be because it was already NO_3^- -depleted from denitrification.

827 The lack of consistent hot moments of CH_4 emissions from the soil despite hydrological conditions in the
 828 subsoil being conducive for CH_4 production could indicate that redox potential is elevated due to presence of for
 829 example NO_3^- . This hypothesis remains to be tested.

830 Per square meter, the ditch emitted less N_2O and CO_2 than the peat soil, but was a hotspot of CH_4 emission,
 831 although annual emissions ($10.4 \text{ g CH}_4 \text{ m}^{-2} \text{ y}^{-1}$) are lower than previously reported for ditches in peat soil (up to
 832 $44 \text{ g CH}_4 \text{ m}^{-2} \text{ y}^{-1}$) (Peacock et al. 2021). For the ditch CH_4 budget, ebullition only constitutes 3.7% of annual net
 833 CH_4 emissions. This proportion may be underestimated as the count of ebullition events may have been
 834 underestimated (Prairie and del Giorgio 2013).

835 **Table 3: Annual summarized budget of, CO_2 ($\text{g CO}_2 \text{ m}^{-2} \text{ y}^{-1}$), CH_4 ($\text{g CH}_4 \text{ m}^{-2} \text{ y}^{-1}$) and N_2O ($\text{g N}_2\text{O m}^{-2} \text{ y}^{-1}$) and**
 836 **converted to global warming potential over a 100 year time scale (GWP₁₀₀) using GWP factors of 273 and 27 for N_2O**
 837 **and CH_4 , respectively, for peat soil and the ditch.**

<i>Peat soil</i>	CO_2^1	CH_4^2	N_2O^2
Annual sum ($\text{g m}^{-2} \text{ y}^{-1}$)	3632 [2941;4347]	0.09 [-0.05;0.22]	41.6 [9.2;14.1]
GWP100 ($\text{tCO}_2\text{-eq ha}^{-1} \text{ y}^{-1}$)	36 [29;43]	0.023 [-0.014;0.06]	32 [25;39]
%GWP	53	0	47
<i>Ditch</i>			
Annual sum ($\text{g m}^{-2} \text{ y}^{-1}$)	974	10.4	0.42
GWP100 ($\text{tCO}_2\text{-eq ha}^{-1} \text{ y}^{-1}$) ³	9.7	2.8 (8.7)	1.1

838 %GWP²

839 70 (50)

22 (44)

8 (6)

²CO₂ = R_n + R_{auto}. Net ecosystem productivity (NEP) input is not included.³Global warming potential (GWP) (100 year) for N₂O = 273 and CH₄ = 27. ³Budget for 20 years GWP for CH₄ = 84 is shown in parenthesis.

840 **4 Data availability**

841 Data for this publication is available for download via

842 <https://dataverse.deic.dk/previewurl.xhtml?token=abda26d4-a430-4830-ad30-fbf5ff1d352e> (Skov Nielsen et al.
843 2025).

844

845 **5 Conclusion**

846 The dataset presented here is unique for temperate fens and demonstrate the advantage of using automated GHG
847 measurements systems to resolve temporal and spatial patterns of GHG dynamics in high detail. The dataset also
848 ~~links demonstrate how especially~~ temporal variation of soil hydrology and temperature is linked to the dynamics
849 of fluxes and highlight that spatial variability in hydrology and temperatures not necessarily ~~is the best predictor~~
850 ~~can be used to predict of~~ flux magnitudes within the sites. The cause for the spatial variability of GHG fluxes
851 remains unresolved ~~and do not clearly link directly to either WTD, soil temperature and soil/groundwater~~
852 ~~chemical parameters. Interestingly it appears that the temporal variability of GHG fluxes across the transect is~~
853 ~~lower than the spatial variation.~~

854 ~~The data only represents one full year in 2022-2023 and hence must be considered specific for this period. It~~
855 ~~must therefore be expected that the annual budget of all GHG's in other years will be different due to other~~
856 ~~climatic and hydrological conditions.~~

857 ~~The initial harvest and herbicide application represent ecosystem disturbances that potentially can alter soil~~
858 ~~biogeochemistry, but they were done months prior to the start of the flux measurements and hence the direct~~
859 ~~effect of herbicide would be minimal. The continued plant removal from inside collars was necessary for the~~
860 ~~flux measurements with the consequence that our fluxes may only be regarded as net soil GHG fluxes, and not~~
861 ~~as being representative of the net ecosystem exchange. Excluding the influence of vegetation have influenced~~
862 ~~the measured fluxes of soil respiration (e.g. excluding root exudates etc.) and reduced plant mediated CH₄ and~~
863 ~~N₂O emissions and lowered most likely also reduced interannual variability. However, the data set represents a~~
864 ~~unique ability to continue to develop models that predict the soil GHG fluxes in response to soil temperature and~~
865 ~~hydrology (WTD) that can aid in prediction of reliable budgets for sites.~~

866 The measurements of the soil GHG fluxes show that the magnitude of annual cumulative CO₂ fluxes are in the
867 same range as in other studies of temperate fens, and that ~~temporal variability magnitudes~~ are largely governed
868 by the seasonality of WTD and ST. ~~However, spatial variation of cumulative fluxes for all GHG were not~~
869 ~~directly related to WTD levels, contradicting the general assumption that WTD is the primary driver of GHG~~
870 ~~emissions.~~ Cumulative soil N₂O fluxes exceed what has been previously reported for temperate fens, but show
871 similar seasonal regulation by ST. However, in contrast to soil CO₂ fluxes, soil N₂O is emitted largely in pulses
872 related to rapid fluctuations of WTD that increase in size with temperature. These measurements therefore point
873 to an important, but difficult to capture dynamic of N₂O in peatlands where hot moments during the warm
874 periods determine most of the annual emissions. A likely cause for the high soil N₂O emissions could be ~~a~~
875 ~~combination of~~ -leaching of inorganic nitrogen from surrounding agricultural fields ~~and release of organic N~~
876 ~~from the decomposing peat, but this remains to be proven.~~ The site was during ~~the~~ measurement period an
877 insignificant source of soil CH₄, which is likely due to the well-drained summer period ~~and~~ a cold wet winter
878 ~~and presence of the major electron acceptors (NO₃⁻, SO₄²⁻ and Fe³⁺),~~ providing suboptimal conditions for CH₄
879 production. ~~However, it cannot be ruled out that the vegetation removal impeded CH₄ emissions, as we~~
880 ~~effectively restricted plant mediated CH₄ emissions. Therefore, caution should be taken when comparing the~~
881 ~~CH₄ flux data to other drained peatlands.~~ Soil CO₂ and N₂O fluxes both showed diurnal variability with higher
882 fluxes during midday where the amplitude between night and day was augmented with ST. This was not
883 observed for soil CH₄ fluxes. The ditch at the site was a net source of both N₂O and CO₂, but at rates 27 and 4

884 times lower than the soil GHG fluxes respectively. However, the ditch acted as a CH₄ source mostly comprised
885 of diffusive emissions from the water surface, but with observations of ebullition.

886 We wish to publish this dataset to the research community with the intention that experimentalists and modellers
887 can use the data to test hypothesis on basic hydrological and thermal regulation of GHG fluxes and develop
888 models to predict spatiotemporal variability of the GHG fluxes.

889 **Competing interests**

890 The authors declare that they have no conflict of interest.

891 **Author contributions**

892 JRC, PEL and KSL designed the experiment and carried them out. ASN performed flux calculation and quality
893 checking. RJP and PEL installed the equipment for groundwater measurements. All authors contributed to
894 writing of this manuscript.

895 **Acknowledgements**

896 The measurements are the results of the RePeat (grant nr. 33010-NIFA-19-724), INSURE and ReWet (grant nr.
897 5229-0002b) projects hosted by University of Copenhagen and Aarhus University. ReWet is part of the Danish
898 roadmap for research infrastructure funded by The Danish Agency for Science and Higher Education. INSURE
899 was part of EJP Soil and received funding from the European Union's Horizon 2020 research and innovation
900 programme under the grant agreement no. 862695.

901 **References**

902 Anthony TL, Silver WL (2023) Hot spots and hot moments of greenhouse gas emissions in agricultural
903 peatlands. *Biogeochemistry* 167:461–477. <https://doi.org/10.1007/s10533-023-01095-y>

904 Askaer L, Elberling B, Friberg T, et al (2011) Plant-mediated CH₄ transport and C gas dynamics
905 quantified in-situ in a Phalaris arundinacea-dominant wetland. *Plant Soil* 343:287–301.
906 <https://doi.org/10.1007/s11104-011-0718-x>

907 Boonman J, Buzacott AJ V, van den Berg M, et al (2024) Transparent automated CO₂ flux chambers
908 reveal spatial and temporal patterns of net carbon fluxes from managed peatlands. *Ecol Indic*
909 164:112121. <https://doi.org/https://doi.org/10.1016/j.ecolind.2024.112121>

910 Brændholt A, Steenberg Larsen K, Ibrom A, Pilegaard K (2017) Overestimation of closed-chamber soil
911 CO₂ effluxes at low atmospheric turbulence. *Biogeosciences* 14:1603–1616.
912 <https://doi.org/10.5194/bg-14-1603-2017>

913 Evans CD, Peacock M, Baird AJ, et al (2021) Overriding water table control on managed peatland
914 greenhouse gas emissions. *Nature* 593:548–552. <https://doi.org/10.1038/s41586-021-03523-1>

915 Hutchinson GL, Mosier AR (1981) Improved Soil Cover Method for Field Measurement of Nitrous
916 Oxide Fluxes. *Soil Science Society of America Journal* 45:311.
917 <https://doi.org/10.2136/sssaj1981.03615995004500020017x>

918 Jørgensen CJ, Struwe S, Elberling B (2012) Temporal trends in N₂O flux dynamics in a Danish wetland
919 - effects of plant-mediated gas transport of N₂O and O₂ following changes in water level and

920 soil mineral-N availability. *Glob Chang Biol* 18:210–222. <https://doi.org/10.1111/j.1365-2486.2011.02485.x>

922 Jørgensen MS, Plauborg F, Kørup K (2023) Climate normal for Foulum 1991-2020. Aarhus University

923 Kandel TP, Lærke PE, Elsgaard L (2018) Annual emissions of CO₂, CH₄ and N₂O from a temperate

924 peat bog: Comparison of an undrained and four drained sites under permanent grass and

925 arable crop rotations with cereals and potato. *Agric For Meteorol* 256–257:470–481.

926 <https://doi.org/10.1016/j.agrformet.2018.03.021>

927 Koch J, Elsgaard L, Greve MH, et al (2023) Water-table-driven greenhouse gas emission estimates

928 guide peatland restoration at national scale. *Biogeosciences* 20:2387–2403.

929 <https://doi.org/10.5194/bg-20-2387-2023>

930 Köhn D, Welpelo C, Günther A, Jurasinski G (2021) Drainage Ditches Contribute Considerably to the

931 CH₄ Budget of a Drained and a Rewetted Temperate Fen. *Wetlands* 41:71.

932 <https://doi.org/10.1007/s13157-021-01465-y>

933 Kroon PS, Hensen a., Bulk WCM, et al (2008) The importance of reducing the systematic error due to

934 non-linearity in N₂O flux measurements by static chambers. *Nutr Cycl Agroecosyst* 82:175–186.

935 <https://doi.org/10.1007/s10705-008-9179-x>

936 Nguyen DB, Rose MT, Rose TJ, et al (2016) Impact of glyphosate on soil microbial biomass and

937 respiration: A meta-analysis. *Soil Biol Biochem* 92:50–57.

938 <https://doi.org/https://doi.org/10.1016/j.soilbio.2015.09.014>

939 Nielsen CK, Liu W, Koppelgaard M, Laerke PE (2024) To Harvest or not to Harvest: Management

940 Intensity did not Affect Greenhouse Gas Balances of Phalaris Arundinacea Paludiculture.

941 *Wetlands* 44:79. <https://doi.org/10.1007/s13157-024-01830-7>

942 Padilla JT, Selim HM (2020) Environmental behavior of glyphosate in soils. *Advances in Agronomy*

943 159:1–34. <https://doi.org/10.1016/BS.AGRON.2019.07.005>

944 Peacock M, Audet J, Bastviken D, et al (2021) Small artificial waterbodies are widespread and

945 persistent emitters of methane and carbon dioxide. *Glob Chang Biol* 27:5109–5123.

946 <https://doi.org/10.1111/gcb.15762>

947 Pedersen AR, Petersen SO, Schelde K (2010) A comprehensive approach to soil-atmosphere trace-

948 gas flux estimation with static chambers. *Eur J Soil Sci* 61:888–902.

949 <https://doi.org/10.1111/j.1365-2389.2010.01291.x>

950 Pihlatie MK, Christiansen JR, Aaltonen H, et al (2013) Comparison of static chambers to measure CH₄

951 emissions from soils. *Agric For Meteorol* 171–172:124–136.

952 <https://doi.org/10.1016/j.agrformet.2012.11.008>

953 Prairie YT, del Giorgio PA (2013) A new pathway of freshwater methane emissions and the putative

954 importance of microbubbles. *Inland Waters* 3:311–320. <https://doi.org/10.5268/IW-3.3.542>

955 Pullens JWM, Abalos D, Petersen SO, Pedersen AR (2023) Identifying criteria for greenhouse gas flux

956 estimation with automatic and manual chambers: A case study for N_2O. *Eur J Soil*

957 *Sci* 74: <https://doi.org/10.1111/ejss.13340>

958 Reza Mashhadi S, Grombacher D, Zak D, et al (2024) Borehole nuclear magnetic resonance as a
959 promising 3D mapping tool in peatland studies. *Geoderma* 443:116814.
960 <https://doi.org/10.1016/j.geoderma.2024.116814>

961 Rheault K, Christiansen JR, Larsen KS (2024) goFlux: A user-friendly way to calculate GHG fluxes
962 yourself, regardless of user experience. *J Open Source Softw* 9:6393.
963 <https://doi.org/10.21105/joss.06393>

964 Sø JS, Sand-Jensen K, Martinsen KT, et al (2023) Methane and carbon dioxide fluxes at high
965 spatiotemporal resolution from a small temperate lake. *Science of The Total Environment*
966 878:162895. <https://doi.org/10.1016/j.scitotenv.2023.162895>

967 Tiemeyer B, Freibauer A, Borraz EA, et al (2020) A new methodology for organic soils in national
968 greenhouse gas inventories: Data synthesis, derivation and application. *Ecol Indic* 109:105838.
969 <https://doi.org/10.1016/j.ecolind.2019.105838>

970 Vroom RJE, van den Berg M, Pangala SR, et al (2022) Physiological processes affecting methane
971 transport by wetland vegetation – A review. *Aquat Bot* 182:103547.
972 <https://doi.org/https://doi.org/10.1016/j.aquabot.2022.103547>

973 Wik M, Varner RK, Anthony KW, et al (2016) Climate-sensitive northern lakes and ponds are critical
974 components of methane release. *Nat Geosci* 9:99–105. <https://doi.org/10.1038/ngeo2578>

975

976 Wilson SJ, Bond-Lamberty B, Noyce G, et al (2024) fluxfinder: An R Package for Reproducible
977 Calculation and Initial Processing of Greenhouse Gas Fluxes From Static Chamber
978 Measurements. *J Geophys Res Biogeosci* 129:. <https://doi.org/10.1029/2024JG008208>

979